

Interpretable Evaluation of AI-Generated Content with Language-Grounded Sparse Encoders

Yiming Tang¹, Arash Lagzian¹, Srinivas Anumasa¹, Qiran Zou¹,
Trang Nguyen², Ehsan Adeli², Ching-Yu Cheng¹, Yilun Du³,
Dianbo Liu^{†1}

¹National University of Singapore.

²Stanford University.

³Harvard University.

Contributing authors: yiming@nus.edu.sg; dianbo@nus.edu.sg;

Abstract

While the quality of AI-generated contents, such as synthetic images, has become remarkably high, current evaluation metrics provide only coarse-grained assessments, failing to identify specific strengths and weaknesses that researchers and practitioners need for model selection and development, further limiting the scientific understanding and commercial deployment of these generative models. To address this, we introduce Language-Grounded Sparse Encoders (LanSE), a novel architecture that creates interpretable evaluation metrics by identifying interpretable visual patterns and automatically describing them in natural language. Through large-scale human evaluation (more than 11,000 annotations) and large multimodal model (LMM) based analysis, LanSE demonstrates reliable capabilities to detect interpretable visual patterns in synthetic images with more than 93% accuracy in natural images. LanSE further provides a fine-grained evaluation framework that quantifies four key dimensions of generation quality, prompt match, visual realism, physical plausibility, and content diversity. LanSE reveals nuanced model differences invisible to existing metrics, for instance, FLUX’s superior physical plausibility and SDXL-medium’s strong content diversity, while aligning with human judgments. By bridging interpretability with practical evaluation needs, LanSE offers all users of generative AI models a powerful tool for model selection, quality control of synthetic content, and model improvement. These capabilities directly address the need for public confidence and safety in AI-generated content, both critical for the future of generative AI applications.

Introduction

AI-synthesized contents created by generative machine learning models is increasingly used in various aspects of society, including artistic design, advertisement generation, and video production. While recent generative models are remarkably fluent in producing highly realistic outputs [1, 2], they are still prone to notable failure modes, such as hallucinating nonexistent objects [3], misusing lighting cues [4], and violating anatomical coherence [5]. When AI trains on AI-generated content, these failures cascade through systems; for example, medical AI learning from synthetic images with anatomical errors perpetuates those mistakes in real diagnoses [6]. Therefore, it is vital to measure quality of data generated by AI, identify and remove these failures before releasing them for applications and to the public. However, there exists a significant gap in evaluating the quality of generated content and its alignment with human intent. While methods for AI-synthesized data evaluation, typically based on semantic similarity [7], distributional alignment [8, 9], or aesthetics [10], can capture certain aspects of quality, they lack the granularity and interpretability needed to provide nuanced assessments on varied model performance axis [11, 12]. These significant gaps in evaluation can mislead model selection and mask critical failure modes, where models with higher metric scores can still generate outputs with unacceptable structural errors or physics violations [13, 14]. Recent analyses have shown that the fundamental problem of current evaluation approaches is they directly utilize high-dimensional embedding spaces that contain biased information and can ignore critical visual patterns [15, 16].

Unlike many existing evaluation methods that conduct a holistic assessment and assign a single score to each generated output, humans evaluate visual content by identifying distinct visual patterns and considering them collectively [17–22]. Consider how art critics work: when evaluating a painting created from a prompt, they rarely assign a single score. Instead, they describe which aspects work and which fail: the lighting may be striking, the composition balanced, the anatomy flawed. Previous studies in human cognition have shown that people rely on specific visual cues when judging image quality—such as facial asymmetry [23], inconsistent lighting or shadows [24], and unnatural textures [25]. However, such factors are typically overlooked by existing evaluation metrics, which reduce assessment to single scores or opaque embeddings. This disconnect highlights the urgent need for evaluation methods grounded in interpretable visual patterns, better aligned with how humans assess visual content.

To automatically identify such interpretable visual patterns needed for AI-synthesized image evaluation, recent advances in mechanistic interpretability [26, 27] offer useful tools. Studies have shown that enforcing sparsity on various neural modules elicits monosemantic neurons—individual units that only respond to certain specific concepts [28]. In detail, the linear representation hypothesis [29] reveals that these meaningful features are often encoded as directions in representation space, and modules like sparse autoencoders [30] and transcoders [31] can effectively extract them. Crucially, recent works have found that such interpretable features often correlate with specific failure patterns in generative models [32]. This motivates us to adapt the interpretability modules for evaluation, creating metrics that are both rigorous in computation and interpretable in language to close the gap in evaluating AI generated contents.

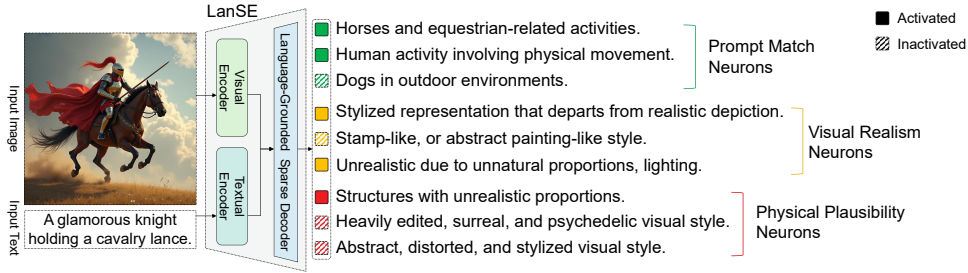


Fig. 1: Language-Grounded Sparse Encoders (LanSE). Given an input image-caption pair, LanSE maps visual and textual inputs into a sparse, interpretable feature space that reflect evaluation dimensions. LanSE neurons are categorized according to their interpretable visual patterns. Only a few neurons are activated per input.

To solve the problems above, we introduce Language-Grounded Sparse Encoders (LanSE), a method that automatically learn thousands of interpretable visual patterns from training data and use these visual patterns to conduct fine-grained evaluation of synthetic images produced by generative machine learning models (Figure 1). By automatically collecting and concatenating neurons from trained interpretability modules, LanSE filters out noisy neurons, and keeps only the most reliable neurons that serve as high-accuracy visual quality indicators. The semantic meaning of each neuron, which we refer to as an interpretable visual pattern, is automatically identified and phrased by large multimodal models (LMMs). Through extensive human evaluation involving over 11,000 annotations from four independent annotators, LanSE demonstrates a reliable ability to detect nuanced visual patterns, achieving over 93% agreement with human judgments. In addition to natural images, we extended our evaluation pipeline to medical imaging.

Leveraging these interpretable features, LanSE provides a comprehensive evaluation framework that assesses generative models along four critical dimensions: prompt match (whether concepts in prompts exist in images [33]), visual realism (photorealism of generated content [34]), physical plausibility (adherence to intuitive physics constraints [35]), and content diversity (variation in generated outputs [36]). LanSE metrics decompose generative model quality into interpretable dimensions, revealing critical aspects that traditional existing metrics fail to capture or even contradict. To our best knowledge, LanSE provides the first automatic evaluation method for intuitive physics violations, the first semantic alignment metrics and content diversity metrics that support assessments on targeted semantic groups.

By bridging mechanistic interpretability with practical evaluation needs, LanSE improves how we assess generative models today and lays the foundation for more trustworthy, controllable, and safer systems. Its LMM-driven automated pipeline scales the curation of interpretable visual patterns beyond what manual annotation can support. Beyond image generation, LanSE offers a generalizable, interpretable evaluation framework for video synthesis, reinforcement learning, and autonomous-driving perception. The same capacity to extract fine-grained, language-grounded features translates to scientific domains, biomedical imaging, remote sensing, and physics-based

simulation, where rigorous quality control is essential. By making model behavior more explainable and reliable, LanSE can strengthen public confidence and safety in AI across education, healthcare, and digital media.

Results

We introduce Language-Grounded Sparse Encoders (LanSE), a general framework for evaluating visual generative models. LanSE detects and names specific visual patterns, such as objects, textures, or structural errors, in synthetic images, whether produced from a text prompt, other inputs, or without any condition. It identifies more than 5,000 such patterns with high reliability, showing strong agreement with over 10,000 human annotations from four independent annotators. From these patterns, we derive four detailed evaluation measures: prompt match (faithfulness to the conditioned description), visual realism (photographic quality), physical plausibility (adherence to the rules of physics), and content diversity (variety of outputs). These measures were validated against more than 3,000 additional human annotations, showing high consistency with human judgment. We then use LanSE to benchmark eight recent generative models of different designs and sizes, revealing clear strengths, weaknesses, and similarities between models—insights that can guide model development and selection. Finally, we compare LanSE with common existing metrics such as FID, CLIP score, and Inception score, showing that LanSE can detect important quality differences missed by these methods.

LanSE Automatically Detects and Names Five Thousand Visual Patterns in Synthetic Images

Modern generative machine learning models learn fine-grained information in a special space within the model encoding interpretable patterns [37, 38]. Various interpretability methods, such as sparse autoencoders [39, 40], transcoders [41], and crosscoders [42] have been introduced to identify these interpretable patterns [43]. However, without careful curation, these identified patterns are often noisy and activating on unrelated patterns and undermining their interpretability [44, 45].

To address this challenge, we develop LanSE, which finds visual patterns in images generated by machine learning models. It does this by collecting millions of candidate neurons from interpretation modules, using LMMs to describe the patterns each neuron detects, and keeping only those with high accuracy (Figure 2).

LanSE uses LMMs to systematically curate neurons at scale. It begins by aggregating neurons from 250 interpretability modules trained on diverse datasets, producing 3.75 million candidates. In a two-stage process, LMMs first examine each neuron’s most strongly activated images to generate a natural language description of the visual pattern it detects. Neurons are then filtered by their measured accuracy, keeping only those that match their described pattern more than 80% of the time (see Method).

This process yields 5,309 high-quality neurons, each corresponding to a distinct visual pattern found in synthetic images. These patterns are grouped into nine categories: semantic content—(1) human, (2) animal, (3) object, (4) activity, (5) environment; unrealistic patterns—(6) style, (7) artifact; and physics violations—(8)

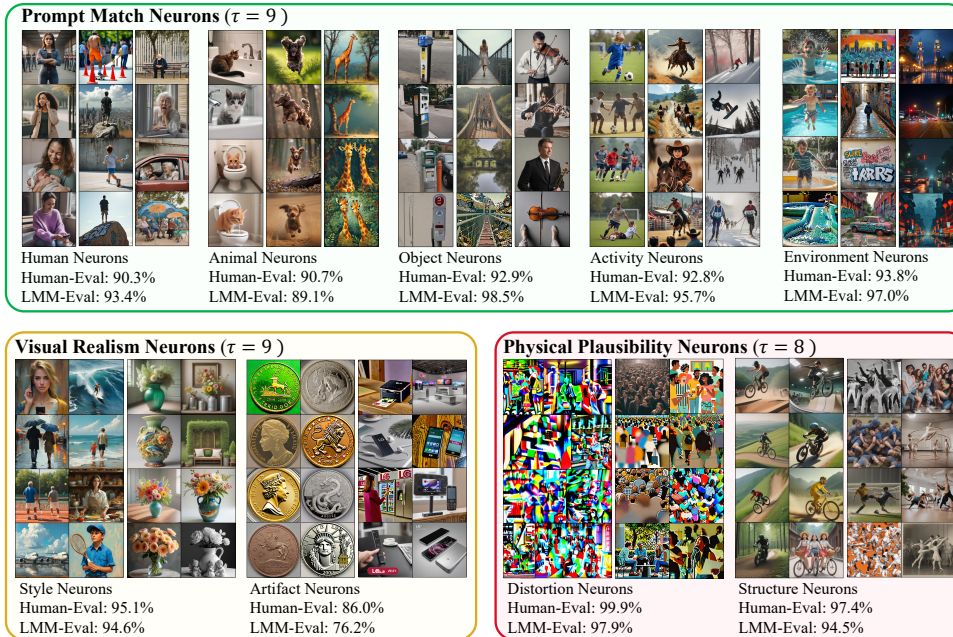


Fig. 2: LanSE neurons and their Human/LMM evaluations. For each of the neuron groups, we randomly sampled 1,000 samples from all the input-neuron pairs with the inputs able to activate the neuron. A total of more than 11,000 human annotations from four independent human annotators, along with 18,000 annotations from two LMMs were collected to determine LanSE’s accuracies.

distortion, (9) structure. Each category plays a specific role in LanSE’s evaluation framework (examples in Appendix A).

Visual Patterns Identified by LanSE Align with Human Annotations

To understand if the visual patterns detected by LanSE are both accurate and reliable for evaluating image quality, we validated them against large-scale human and automated assessments. We conducted evaluations involving over 11,160 human annotations from four independent annotators (see Appendix F). Each human annotator reviewed 2,790 neuron–image pairs, where each pair comprised a neuron’s interpreted description and an image that activated it, and judged whether the activation matched the described pattern. As shown in Figure 2, LanSE neurons achieved 93% accuracy under human evaluation, with category-specific performance ranging from 76% to 99%. The four annotators achieved an inter-annotator agreement of 85.93%. In addition to human annotation, we also included automated assessments from two state-of-the-art large multimodal models (LMMs). On the same dataset, automated evaluation of

LanSE show strong agreement with human annotation achieving 90.4% accuracy with category-specific performance ranging from 77.3% to 98.7%.

Derivation of Diagnostic Metrics for Evaluating Synthetic Images Using Visual Patterns Identified by LanSE

Having introduced LanSE and validated the quality of its detected visual patterns, we now show how these patterns induce four diagnostic metrics for synthetic-image quality: *prompt match*, *visual realism*, *physical plausibility*, and *content diversity* (See Appendix E). These metrics target complementary aspects that common aggregate measures fail to distinguish. Figure 3 summarizes the computations.

Formally, let $\text{LanSE}(x, y) = \mathbf{n} = [n_1, \dots, n_d] \in \{0, 1\}^d$ denote the sparse activation vector for an image-text pair (x, y) . Each neuron n_i is associated with a natural-language explanation ϵ_i (e.g., “horses and equestrian-related activities”). The d neurons are partitioned into 3 disjoint groups ($\mathcal{C} = \mathbf{prompt, real, phy}$). For $g \in \mathcal{C}$, we write $N_g(x, y) \in \{0, 1\}^{d_g}$ for the subvector of activations in group g .

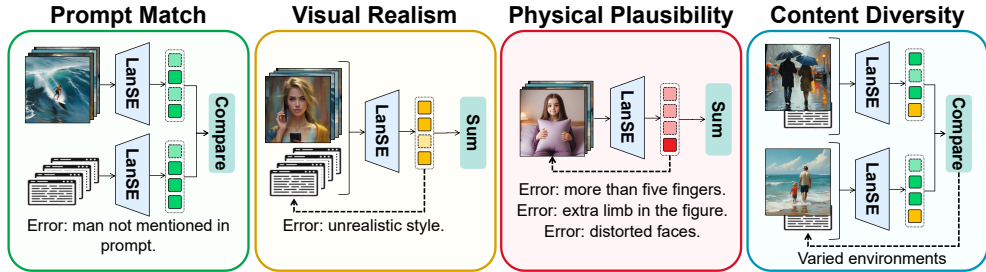


Fig. 3: Evaluation metrics based on LanSE neurons. We define four evaluation metrics utilizing the activations of LanSE’s interpretable neuron groups. They each measure a distinct aspect of generative model’s performances.

Prompt mismatches occur when models fail to faithfully generate content based on the prompts. This can stem from hallucinated or omitted elements [46]. Images with severe prompt mismatches are often undesirable and unsuitable for model fine-tuning [47]. To measure this, we introduce the prompt match metric, which quantifies the divergence between neuron activations prompted by visual and textual modalities: $\mathcal{M}_{\mathbf{prompt}}(\mathcal{X}, \mathcal{Y}) = \mathbb{E}_{\mathbf{D}} \|\mathbf{N}_{\mathbf{prompt}}^v(\mathbf{x}) \oplus \mathbf{N}_{\mathbf{prompt}}^t(\mathbf{y})\|_1$, where $\mathbf{N}_{\mathbf{prompt}}^v(x)$ and $\mathbf{N}_{\mathbf{prompt}}^t(y)$ are the activations for single-modality LanSEs onto the same latent space.

Visually unrealistic outputs occur when generative models produce patterns that make images photographically implausible. These can include intentional stylistic effects, such as a watercolor style [48], as well as unintended artifacts, such as repetitive prompt-induced patterns that deviate from real-world conventions [49]. To quantify such deviations, we propose the visual realism metric, which measures the activation of neurons associated with both styles and artifacts: $\mathcal{M}_{\mathbf{real}}(\mathcal{X}, \mathcal{Y}) = \mathbb{E}_{\mathbf{D}} \|\mathbf{N}_{\mathbf{real}}(\mathbf{x}, \mathbf{y})\|_1$.

Physical implausibility refers to error patterns in generated images that violate physical principles. These include distorted surfaces and anatomically impossible

structures, such as hands with more than five fingers [5, 50]. Although often subtle, such errors represent critical failure modes that directly undermine the practical usability of generated images. To capture these violations, we define the physical plausibility metric, which quantifies the presence of such errors: $\mathcal{M}_{\text{phy}}(\mathcal{X}, \mathcal{Y}) = \mathbb{E}_{\mathbf{D}} \|\mathbf{N}_{\text{phy}}^{\mathbf{y}}(\mathbf{x})\|_1$.

Content diversity captures the degree of variation in outputs produced by a generative model [51]. Recent research has emphasized the importance of models being creative and generating diverse content [52, 53]. We consider prompt match neurons (e.g., human, animal, object, activity, environment) and style neurons as content-relevant neurons and compute the content diversity metric using the normalized divergence between two samples: $\mathcal{M}_{\text{con}}(\mathcal{X}, \mathcal{Y}) = \mathbb{E}_{\mathbf{D}} \frac{\|\mathbf{N}_{\text{con}}(\mathbf{x}_i, \mathbf{y}_i) \oplus \mathbf{N}_{\text{con}}(\mathbf{x}_j, \mathbf{y}_j)\|_1}{\|\mathbf{N}_{\text{con}}(\mathbf{x}_i, \mathbf{y}_i)\|_1 \cdot \|\mathbf{N}_{\text{con}}(\mathbf{x}_j, \mathbf{y}_j)\|_1}$.

Diagnostic Metrics from LanSE Align with Human Judgments

To assess whether the diagnostic metrics automatically derived from LanSE meaningfully capture quality distinctions in synthetic images, we performed meta-evaluations comparing each metric against human judgments. For the first three metrics—prompt match, visual realism, and physical plausibility—we constructed dedicated validation sets and labeled them using human annotators. Human evaluation of content diversity requires nuanced expertise to assess differences across output distributions and was therefore excluded from this validation.

The validation protocol was as follows: from a pool of 3,000 generated images, two independent annotators classified each image for each metric category as positive (containing the corresponding error type) or negative (error-free). An image was assigned to the positive set if the annotator indicated the presence of the relevant error. We then computed the average metric scores for the positive and negative sets to assess discriminative power. Our results shown in Figure 4 demonstrate strong alignment between LanSE metrics and human judgments. Across all three metrics, images in the negative sets show significantly lower diagnostic metrics than those in the positive sets.

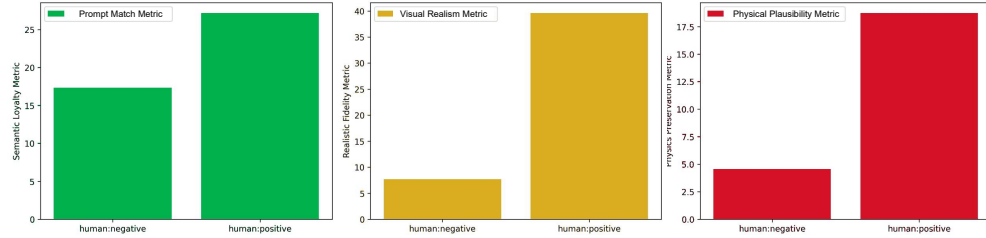


Fig. 4: Validation of LanSE metrics against human judgments. Comparison of average metric values between positive (error-present) and negative (error-free) image sets as classified by human annotators and LMMs. Shown here for visual realism metric across natural images, generated images, and subsets classified by error type. Significant separation between positive and negative sets validates metric effectiveness.

Evaluation of Generative Models Using Diagnostic Metrics from LanSE

Having developed the LanSE method for automatic detection of visual patterns and for deriving diagnostic metrics from these patterns, we next evaluate the quality of synthetic images produced by eight generative models. These include four variants from the Stable Diffusion family, SDXL-turbo, SDXL-base, SDXL-medium, and SDXL-large [54], as well as DALL-E 3 [55], FLUX [56], Kolors [57], and Stable-Cascade [58].

Our results presented in Figure 5 reveal distinct performance profiles for each model. FLUX achieves the highest physical plausibility scores, making it particularly suitable for applications requiring strict physical plausibility. SDXL-medium excels in both photorealism and content diversity, producing the most realistic and varied outputs. DALL-E 3 demonstrates superior prompt match but at the cost of reduced output diversity. Interestingly, we observe that generated images generally exhibit stronger semantic alignment with their captions than real-world image-caption pairs, suggesting that current models may be over-optimized for prompt match. Furthermore, our results reveal a clear correlation between model scale and physical plausibility, larger models significantly reduce distortion and structure errors. Figure 6 presents detailed group-wise performance metrics that enable more nuanced model selection. These fine-grained insights provide practitioners with actionable guidance for choosing models based on their specific application requirements, whether prioritizing prompt match, visual realism, physical plausibility or content diversity.

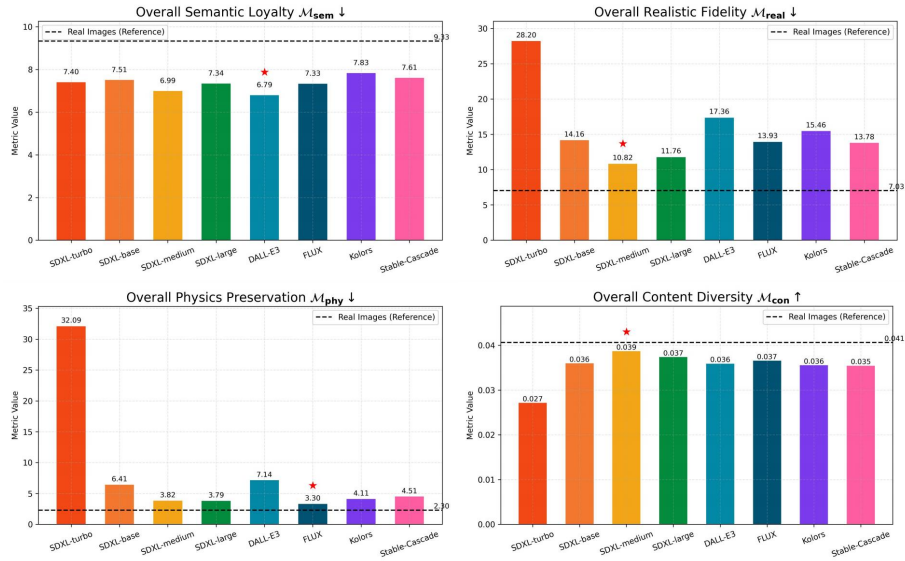


Fig. 5: Evaluation results for generative models. Performance comparison of eight generative models across four LanSE metrics: prompt match, visual realism, physical plausibility, and content diversity. Lower scores indicate better performance for the first three metrics, while higher scores indicate better content diversity.

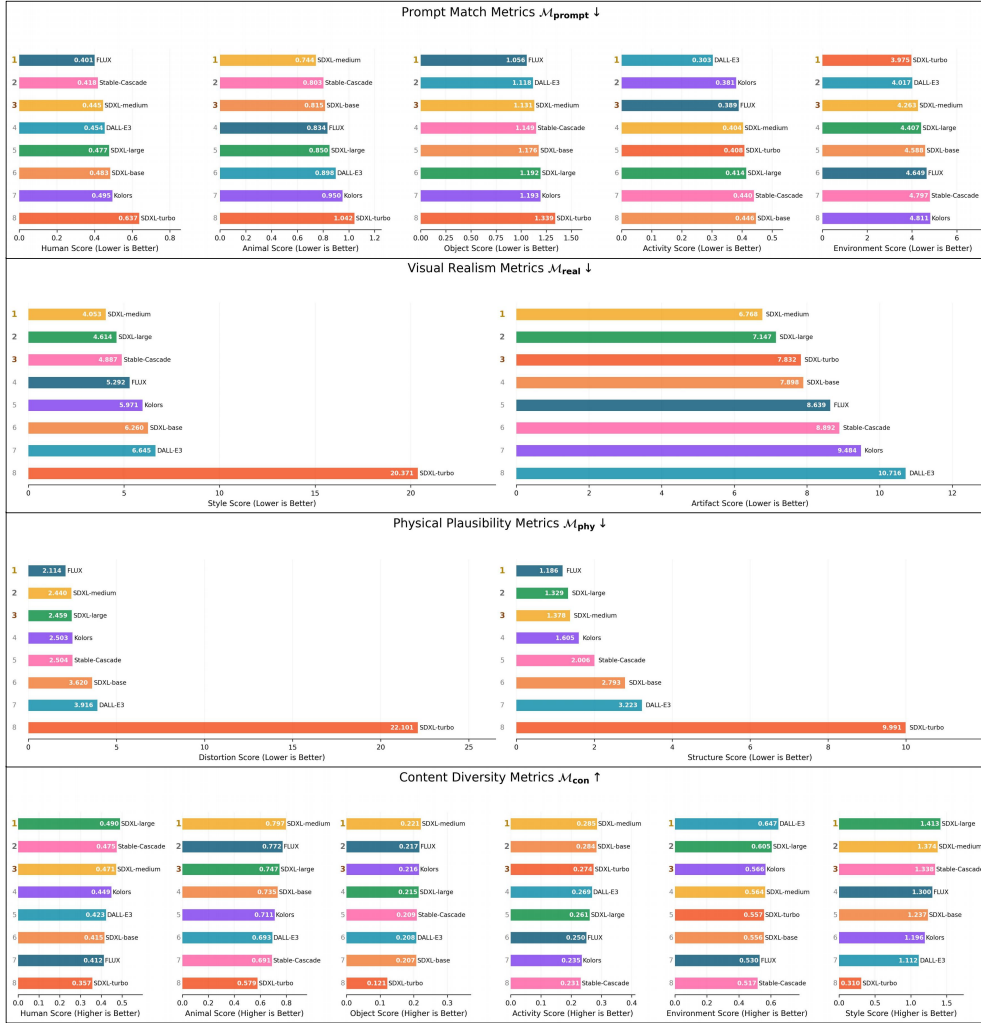


Fig. 6: Model leaderboards for group-wise scores. Different generative models exhibit distinct performance profiles across evaluation dimensions. For prompt match, environmental elements represent the most common source of semantic misalignment across all models. FLUX achieves superior performance in human and object semantics, while SDXL-medium excels at animal semantics, DALL·E3 at activity semantics, and SDXL-turbo at environmental semantics. In visual realism metrics, SDXL-medium demonstrates the strongest performance in avoiding both unmentioned art styles and invented visual artifacts, with SDXL-large as the second-best performer. Physical plausibility metrics reveal FLUX as the leading model in preventing both surface distortions and anatomically implausible structures, followed by SDXL-medium and SDXL-large. Content diversity analysis shows complementary strengths: SDXL-large produces the most varied human representations, SDXL-medium generates the greatest diversity in animals, objects, and activities, while DALL·E3 achieves the highest environmental variety, and SDXL-large gives the best style diversity.

Inter-model Correlation Analysis via LanSE

To examine similarity and difference between generative models at the level of neural activation patterns, we analyze the consistency with which different models trigger LanSE neurons. For each model, we generate 6,000 image–caption pairs and compute pairwise correlation matrices of LanSE activations across all nine neuron groups.

Figure 7 reveals two main findings. First, content neurons, covering human, animal, object, activity, environment, and style, exhibit high inter-model correlations (mean $r = 0.74$), whereas error-signaling neurons, artifact, distortion, and structure, show markedly lower correlations (mean $r = 0.31$). This suggests that models tend to converge on semantic representations but diverge substantially in their failure modes. Second, FLUX and SDXL-Medium display notably higher correlations, particularly in style ($r = 0.60$), environment ($r = 0.82$), and activity ($r = 0.76$) neurons, implying shared architectural or training strategies. By contrast, SDXL-Turbo shows the most distinctive activation patterns, with the lowest average style correlation ($r = 0.51$).

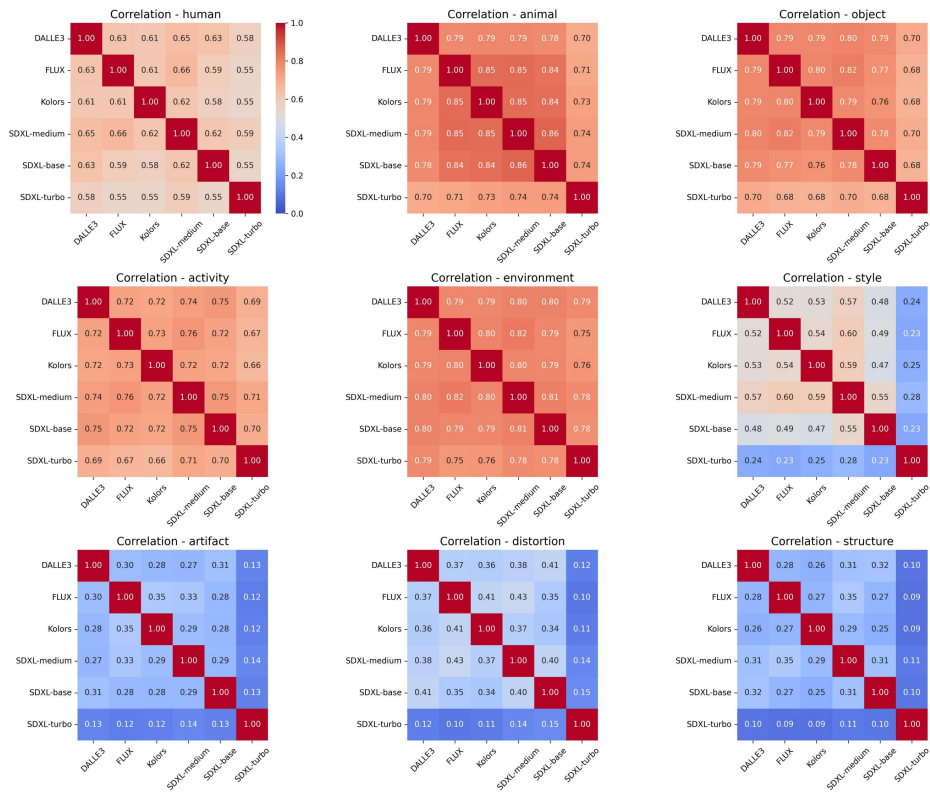


Fig. 7: Conducting correlation analysis on generative models with LanSE. Pairwise correlation matrices computed from LanSE neuron activations across six generative models, with each matrix representing one of nine neuron groups. Warmer colors indicate higher correlation between model pairs.

Comparison of LanSE Metrics with Existing Metrics

To position LanSE within the landscape of generative model evaluation, we compare our metrics with widely-adopted baseline methods: Fréchet Inception Distance (FID) [8], Inception Score (IS) [9], and CLIP Score [59]. Figure 8 reveals several key insights. First, existing metrics show limited discriminative power among recent models. CLIP scores cluster tightly (0.269-0.285), failing to capture the substantial quality differences we observe through LanSE. FID scores, while showing more variation, contradict human preferences, SDXL-base achieves the best FID (6.69) despite producing lower-quality outputs than FLUX or SDXL-medium. This suggests FID’s distributional matching may not align with perceptual quality.

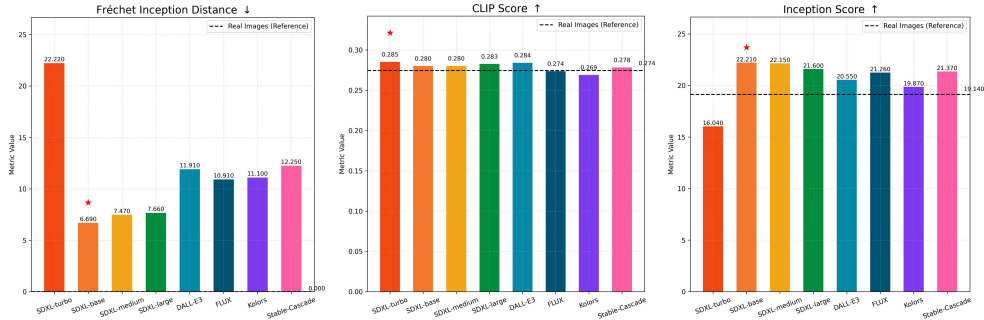


Fig. 8: LanSE reveals model differences that traditional metrics fail to capture. Comparatively, evaluation results across traditional metrics show limited discriminative power and occasional misalignment with human preferences.

To understand these limitations, we conduct detailed analysis comparing CLIP scores with our prompt match metric. While CLIP is widely used for semantic alignment evaluation, it exhibits systematic biases. Figure 9 reveals a critical pattern: image-text pairs with high prompt match errors never achieve high CLIP scores (empty upper-right regions), indicating that severe misalignments are detectable by both metrics. However, the scatter plots show substantial spread in the lower-left regions, where CLIP assigns low scores to images that LanSE identifies as semantically aligned in specific aspects.

This discrepancy stems from CLIP’s bias toward object existence while overlooking compositional details [16]. Figure 10 demonstrates this limitation through examples where CLIP assigns high scores (> 0.28) to images with clear semantic mismatches, unmentioned objects, incorrect activities, or wrong environmental contexts, that LanSE successfully identifies through its specialized neuron groups.

These findings demonstrate that while existing metrics provide useful aggregate measures, they lack the granularity and interpretability needed for actionable model improvement. LanSE’s decomposed evaluation along specific visual patterns enables practitioners to understand not just that models differ, but precisely how and why they differ, critical information for both model selection and development.

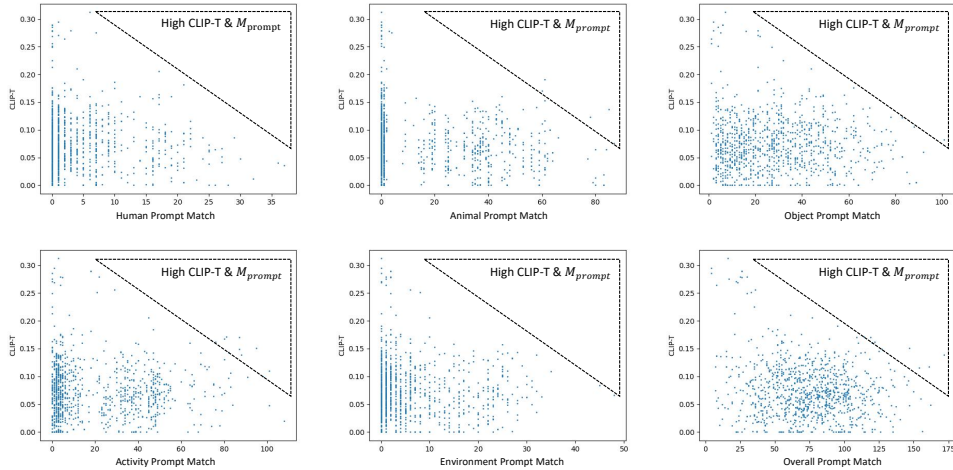


Fig. 9: Clip v.s. M_{prompt} . Each point represents an image–caption pair. Notably, regions with both high CLIP-T and high M_{prompt} are often sparse or unpopulated.

	<p>Prompt: A passenger bus that is making a turn. CLIP Score: 0.2861 (✓) Semantic Mismatches from LanSE: 1. Outdoor nature scenes with trees, vegetation, and human presence. (×) 2. Trees and tree-related elements in natural environments. (×) 3. Outdoor leisure and recreational activities involving water or nature. (×)</p>
	<p>Prompt: A variety of pastries atop a white plate. CLIP Score: 0.2960 (✓) Semantic Mismatches from LanSE: 1. Bedroom or hotel room environments with beds and other furniture. (×) 2. Breakfast or brunch food items. (×) 3. Coffee and coffee-related beverages. (×)</p>
	<p>Prompt: A donut shop is full of different flavors of donuts. CLIP Score: 0.2867 (✓) Semantic Mismatches from LanSE: 1. Technological devices, equipment, and tools. (×) 2. Women participating in various sports and physical activities. (×) 3. Women engaging in various creative or performative activities. (×)</p>
	<p>Prompt: A tennis player holding a tennis racquet while he serves a tennis ball. CLIP Score: 0.2804 (✓) Semantic Mismatches from LanSE: 1. Blue as a dominant or prominent color. (×) 2. Frisbee throwing and catching in outdoor settings. (×) 3. Frisbee-related activities in outdoor/natural settings. (×)</p>

Fig. 10: CLIP’s blind spots revealed through LanSE’s fine-grained analysis. Examples where CLIP assigns high scores (> 0.28) to images with clear semantic mismatches. LanSE successfully detects unmentioned elements that CLIP overlooks.

Discussions

Our results reveal a striking pattern in recent generative models: while they achieve strong semantic alignment, often exceeding that of real-world datasets, they consistently struggle with visual realism, physical plausibility, and content diversity. In particular, recent models frequently exhibit distinctive stylistic signatures that deviate from photorealistic representation, generate distorted surfaces, and produce physically implausible structures. Their content diversity remains significantly below that of natural image distributions. These findings suggest the machine learning community should recalibrate its priorities, shifting focus from semantic alignment, a largely solved problem, toward these more nuanced aspects of visual generation.

From an interpretability perspective, our systematic curation of 5309 interpretable LanSE neurons collected from 3.75 million candidates demonstrates that mechanistic interpretability features can reliably signal visual patterns with over 90% accuracy, forming a robust foundation for evaluating generative models. These features enable targeted assessment of specific quality dimensions while providing decomposed evaluation axes between recent models compared with existing metrics. Rather than treating interpretability features as ancillary tools for post-hoc analysis [60], we propose a paradigm shift: positioning them as structural infrastructure for diagnostic assessment. LanSE’s diverse visual patterns, each grounded in natural language explanations, enable evaluation methods that are not merely quantitative but genuinely explanatory, revealing not just failure rates, but specific failure types and their underlying causes.

Beyond evaluation, LanSE opens several avenues for future development. Looking ahead, researchers should explore expanding LanSE’s scope along multiple dimensions. Task-specific neuron groups could address currently unmeasured qualities such as aesthetic appeal, compositional balance, or social bias. The framework could extend to other generative modalities, with video generation evaluation presenting immediate opportunities for temporal consistency and motion physics assessment. We envision integrating LanSE directly into model training pipelines, where generative models could receive fine-grained feedback through interpretable, feature-level signals. Additionally, LanSE’s architecture naturally supports various downstream applications including multi-label explanation generation [61] (See Appendix B), feature-based information retrieval [62], and systematic slice discovery [63]. By establishing language-grounded sparse encoders as foundational infrastructure, we aim to catalyze a broader transformation in machine learning, one that embraces richer, more interpretable feedback throughout the evaluation, training, and deployment lifecycle.

Limitations

While LanSE provides interpretable and actionable evaluation signals, it is subject to several limitations. First, its ability to assess generative outputs is constrained to visual patterns that are describable in natural language, as neuron validation requires human or LMM-readable explanations. This introduces an anthropocentric bias, subtle, cognitively opaque, or sub-symbolic failure modes may evade detection. Second, LanSE’s reliance on large multimodal models (LMMs) for neuron interpretation may introduce inconsistency or bias into the feature categorization process. Finally, the

scope and quality of evaluation are bounded by the diversity and granularity of the neuron groups discovered. Despite these constraints, we argue that LanSE remains a practical and human-aligned approach: the failure patterns that matter most to end users tend to be those that are both perceptible and articulable. We summarize this guiding philosophy as: "LanSE evaluates with what human language can describe. What we care about, we evolve language to describe." A more detailed discussion of limitations is presented in Appendix I.

Method

In this section, we present the details of our proposed Language-Grounded Sparse Encoders method (See Figure 11). Our method addresses the challenge of transforming mechanistic interpretability features into practical evaluation infrastructure through a systematic three-stage pipeline. It basically proceeds in three stages: (1) discovering sparse latent features using sparsity-driven interpretability modules (2) categorizing these features automatically with the help of large multimodal models (LMMs), and (3) building single-modality LanSEs through a modality distillation procedure to support the computation of prompt match metrics. We extend our method with a human-involved interactive framework that can support the discovery of targeted types of error patterns in Appendix D, which is used to find the distortion group and the structure group of neurons in the LanSEs we have constructed.

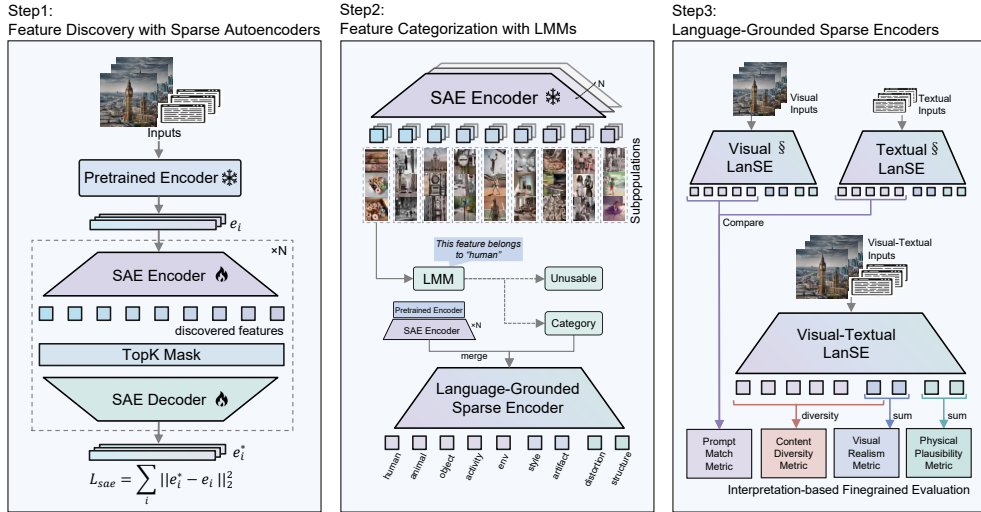


Fig. 11: The general pipeline to construct LanSEs with SAE as the feature discovery tool. §: The Visual LanSE and the Textual LanSE are distilled from the Visual-Textual LanSE, ensuring that the three LanSEs have an aligned latent space.

Dataset Augmentation

For datasets, we have used captions from MSCOCO [64], Flickr8k and Flickr30k [65], TextCaps [66], and NoCaps [67]. We augment these image-caption datasets with generated data using a variety of recently developed generative models [54–57, 68] to get a more diverse range of images with 253,213 images used in total. All of these image-caption datasets are used downstream to construct LanSE models and identify the images that can activate a LanSE neuron.

Automatic Feature Discovery with Sparsity-Driven Interpretability Modules

To discover interpretable patterns, we encode image-caption pairs into embeddings, and use the concatenations of the embeddings to train sparse autoencoders. These sparse autoencoders aim to extract interpretable features from representations with superposition [45], to produce monosemantic neurons [43], latent space neurons that trigger according to a specific concept.

Given the image-caption pairs, $(\mathbf{x}_i, \mathbf{y}_i) \sim \mathbb{P}(\mathcal{X}, \mathcal{Y}), (i = 1, 2, \dots, N)$, we encode them into a joint representation $\mathbf{e}_i \in \mathbb{R}^d$ by concatenating the outputs of two fixed pretrained encoders E_x and E_y :

$$\mathbf{e}_i = [E_x(\mathbf{x}_i), E_y(\mathbf{y}_i)]. \quad (1)$$

Sparse autoencoders are neural networks designed to reconstruct input data while enforcing sparsity in their latent representations, encouraging each neuron to respond to distinct, interpretable features [69]. We subsequently train multiple k -sparse autoencoder [70] each comprised of one encoder $\mathbf{z}_i = \text{Enc}(\mathbf{e}_i) = \text{ReLU}(\mathbf{w} \cdot \mathbf{e}_i + \mathbf{b})$ and one decoder $\text{Dec}(\mathbf{z}_i) = \text{ReLU}(\mathbf{w} \cdot \mathbf{z}_i + \mathbf{b})$ to reconstruct \mathbf{e}_i from a sparse latent vector, $\mathbf{z}_i = \text{Enc}(\mathbf{e}_i)$. To enforce sparsity, we adopt a top- k activation scheme: for each \mathbf{z}_i , we retain only the k highest-magnitude activations and set the rest to zero, yielding the following training objective:

$$\mathcal{L}_{\text{sae}} = \mathbb{E}_{(\mathbf{x}_i, \mathbf{y}_i)} \left[\|\text{Dec}(\text{TopK}(\text{Enc}(\mathbf{e}_i))) - \mathbf{e}_i\|_2^2 \right]. \quad (2)$$

This top- k sparsity constraint has been proven to support identifying monosemantic neurons at scale [69]. Each neuron in the latent space becomes sensitive to a distinct recurring pattern across image-caption pairs ranging from object categories to physics violations, laying the foundation for feature-level analysis in subsequent stages. The activation of a neuron in the trained k -sparse autoencoder is given as:

$$\mathcal{A}_{\text{neuron}}(\mathbf{e}_i) = \text{ReLU}(\mathbf{w}_{\text{neuron}} \cdot \mathbf{e}_i + b_{\text{neuron}}). \quad (3)$$

To capture a wide range of interpretable visual patterns, we train a large ensemble of sparse autoencoders (SAEs), each on a different subset of the dataset. This strategy promotes the diversity of learned visual patterns by ensuring that each SAE learns from a distinct portion of the image distribution. We train in total 200 (could be further scaled up) k -sparse autoencoders using OpenAI’s clip-vit-large-14 model as E_x and E_y [71] ($d = 768$) to find a diverse set of neurons, with each SAE model having a

latent space of 15,000 neurons and $k = 32$ for the top-k sparsity constraint. We have adopted hyperparameters similar to recent advances in the field of mechanistic interpretability [72, 73]. In the exploration stage of this project, we have also tried using other alternative models [74] as the visual encoder but got less interpretable results. We therefore use CLIP models as their visual embeddings are aligned with semantic meaning and supports the finding of more explainable features. We subsequently combine them by collecting their weights from the linear layers, $\mathbf{w}_{\text{neuron}}, b_{\text{neuron}}$.

Feature Categorization with LMMs

After training the sparsity-driven interpretability modules, we obtain a collection of latent neurons, each of these neurons is activated in response to a specific feature. We employ a prompt engineering pipeline that uses large multimodal models (LMMs) [75, 76] to analyze and interpret these latent neurons.

In specific, for each neuron, we collect a subpopulation [77] of image-text pairs that trigger strong activations. We then prompt Claude-3.5-Haiku[75] to summarize the common characteristics within these samples. The prompt we use to summarize the commonality of the feature is given below (more prompts in Appendix C):

Feature Summarization Prompt (Prompt_{sum})

You are an expert in multimodal feature analysis. Given the following images and texts: {samples}, analyze the commonalities among them. Concisely summarize one common feature that is possessed by all the instances. Wrap the commonality in square brackets.

Based on their returned summarization of commonalities, we categorize the features into one of the nine humanly-designed subgroups, \mathbf{C} . These subgroups include five categories designed for semantics: **human**, **animal**, **object**, **activity**, and **environment**; two categories to capture unrealistic artifacts: **style** and **artifact**; and two to capture physics violations: **distortion** and **structure** (See Appendix G). We use the following prompt to categorize the neuron based on their explanations.

Feature Categorization Prompt (Prompt_{cat})

We have a group of datapoints possessing one common feature. Given the description of their explanation: {explanation}, which of the five categories does the feature best belong to, human, animal, object, activity, or environment? Only output the category and wrap the answer in square brackets.

Following notations in previous theoretical analysis on prompt engineering [78], the feature analysis procedures on a LanSE neuron can be formulated as below:

$$\epsilon_n = \text{LMM}(\text{Samples}|\text{Prompt}_{\text{sum}}). \quad (4)$$

$$c_n = \text{LMM}(\epsilon_n|\text{Prompt}_{\text{cat}}) \in \mathbf{C}. \quad (5)$$

Detailed prompts on how we use LMMs for feature analysis are listed in Appendix C. Noticing that the annotations are obtained during the construction of LanSEs, no further assistance are needed from LMMs during evaluation inferences.

Modality Distillation for Language-Ground Sparse Encoders

We denote our visual-textual LanSEs as $S_c : (\mathcal{X}, \mathcal{Y}) \rightarrow \mathbb{R}^{d_c}$, ($c \in \mathbf{C}$). From the trained sparse auto-encoders, we get their weight matrices by concatenating neurons in corresponding neuron groups: $\mathbf{W}_c = [\mathbf{w}_n], \mathbf{b}_c = [b_n]$ ($n \in N_c$).

$$S_c(\mathbf{x}_i, \mathbf{y}_i) = \text{ReLU}(\mathbf{W}_c \cdot [E_x(\mathbf{x}_i), E_y(\mathbf{y}_i)] + \mathbf{b}_c). \quad (6)$$

Subsequently, for the semantic neuron groups (*human, animal, object, activity and environment*), we distill [79] the visual-textual LanSEs, $S_c, c \in \mathbf{C}$, into single-modality LanSEs, S_c^{img} and S_c^{txt} ($c \in \mathbf{C}$). The LanSEs are initialized with pretrained visual and textual encoders and tuned with parameter efficient fine-tuning [80]. In specific, we tune the last layer of the CLIP model and attach a tunable head from the CLIP embedding layer to the sparse latent space. We minimize the L2-norm between the outputs of the modality-specific encoders and their corresponding activations in the joint model:

$$\begin{cases} \mathcal{L}_c^{\text{img}} = \sum_i \|S_c^{\text{img}}(\mathbf{x}_i) - S_c(\mathbf{x}_i, \mathbf{y}_i)\|_2^2, c \in \mathbf{C}. \\ \mathcal{L}_c^{\text{txt}} = \sum_i \|S_c^{\text{txt}}(\mathbf{y}_i) - S_c(\mathbf{x}_i, \mathbf{y}_i)\|_2^2, c \in \mathbf{C}. \end{cases} \quad (7)$$

This modality distillation procedure results in models that can map single-modality inputs, such as image-only or text-only, to the shared sparse latent space, enabling us to apply LanSE even when only images are available, and to analyze which features are encoded in one modality but not the other.

Conclusion

We present LanSE, a novel architecture that enables interpretable, fine-grained evaluation of generative models by indentifying interpretable visual patterns and grounding them in natural language. Built on a large pool of curated interpretable neurons, LanSE offers four actionable metrics, prompt match, visual realism, physical plausibility, and content diversity, that capture key dimensions of generation quality. Extensive human and automated evaluations validate LanSE’s reliability and alignment with human judgment. By bridging mechanistic interpretability with practical evaluation needs, LanSE contributes a robust, human-aligned framework that empowers more transparent, accountable, and controllable generative systems. Our models and evaluation suite are released to support further research and deployment.

Acknowledgements

This research was supported by the National University of Singapore and benefited from access to computational resources provided by CogAI4S. We acknowledge the

potential presence of unintended biases or conflicts of interest, particularly due to the use of LMMs to interpret the visual patterns. We are deeply grateful to the human annotators who contributed their time and expertise to this project, including Yiming Tang, Qiran Zou, Arash Lagzian, Samson Yu, Harshvardhan Saini and Daksh Mor. Their careful assessments played a vital role in the validation of the LanSE framework. We also thank Xuming Ran for his valuable advice and guidance during the initial stages of the project. Finally, we are grateful to Vaishnavh Nagarajan for his insightful feedback and constructive suggestions that helped shape the direction of this work.

References

- [1] Rombach, R., Blattmann, A., Lorenz, D., Esser, P. & Ommer, B. High-resolution image synthesis with latent diffusion models (2022). URL <https://arxiv.org/abs/2112.10752>. 2112.10752.
- [2] Tian, K., Jiang, Y., Yuan, Z., Peng, B. & Wang, L. Visual autoregressive modeling: Scalable image generation via next-scale prediction (2024). URL <https://arxiv.org/abs/2404.02905>. 2404.02905.
- [3] Aithal, S. K., Maini, P., Lipton, Z. C. & Kolter, J. Z. Understanding hallucinations in diffusion models through mode interpolation (2024). URL <https://arxiv.org/abs/2406.09358>. 2406.09358.
- [4] Zhao, Y., Dasari, M. & Guo, T. Clear: Robust context-guided generative lighting estimation for mobile augmented reality (2025). URL <https://arxiv.org/abs/2411.02179>. 2411.02179.
- [5] Narasimhaswamy, S. *et al.* Handdiffuser: Text-to-image generation with realistic hand appearances. Presented at CVPR 2024 (2024). Available at <https://doi.org/10.1109/CVPR52733.2024.00239>.
- [6] Shumailov, I. *et al.* The curse of recursion: Training on generated data makes models forget (2024). URL <https://arxiv.org/abs/2305.17493>. 2305.17493.
- [7] Hessel, J., Holtzman, A., Forbes, M., Bras, R. L. & Choi, Y. Clipscore: A reference-free evaluation metric for image captioning (2022). URL <https://arxiv.org/abs/2104.08718>. 2104.08718.
- [8] Jayasumana, S. *et al.* Rethinking fid: Towards a better evaluation metric for image generation (2024). URL <https://arxiv.org/abs/2401.09603>. 2401.09603.
- [9] Barratt, S. & Sharma, R. A note on the inception score (2018). URL <https://arxiv.org/abs/1801.01973>. 1801.01973.
- [10] Huang, H. *et al.* Predicting scores of various aesthetic attribute sets by learning from overall score labels (2023). URL <https://arxiv.org/abs/2312.03222>. 2312.03222.

- [11] Sampaio, G. G. *et al.* Typescore: A text fidelity metric for text-to-image generative models (2024). URL <https://arxiv.org/abs/2411.02437>. 2411.02437.
- [12] Chen, C., Namboodiri, V. P. & Padget, J. Understanding the vulnerability of clip to image compression (2023). URL <https://arxiv.org/abs/2311.14029>. 2311.14029.
- [13] Bianchi, L., Carrara, F., Messina, N. & Falchi, F. Is clip the main roadblock for fine-grained open-world perception? (2024). URL <https://arxiv.org/abs/2404.03539>. 2404.03539.
- [14] Kirstain, Y. *et al.* Pick-a-pic: An open dataset of user preferences for text-to-image generation (2023). URL <https://arxiv.org/abs/2305.01569>. 2305.01569.
- [15] Zhang, R., Isola, P., Efros, A. A., Shechtman, E. & Wang, O. The unreasonable effectiveness of deep features as a perceptual metric (2018). URL <https://arxiv.org/abs/1801.03924>. 1801.03924.
- [16] Schrodi, S., Hoffmann, D. T., Argus, M., Fischer, V. & Brox, T. Two effects, one trigger: On the modality gap, object bias, and information imbalance in contrastive vision-language models (2025). URL <https://arxiv.org/abs/2404.07983>. 2404.07983.
- [17] Biederman, I. Recognition-by-components: a theory of human image understanding. *Psychological review* **94**, 115 (1987).
- [18] Marr, D. *Vision: A computational investigation into the human representation and processing of visual information* (MIT press, 2010).
- [19] Zeki, S. Art and the brain. *Journal of Consciousness Studies* **6**, 76–96 (1999).
- [20] Clark, H. H. *Using language* (Cambridge university press, 1996).
- [21] Nightingale, S. J., Wade, K. A. & Watson, D. G. Can people identify original and manipulated photos of real-world scenes? *Cognitive research: principles and implications* **2**, 1–21 (2017).
- [22] Farid, H. Creating, using, misusing, and detecting deep fakes. *Journal of Online Trust and Safety* **1** (2022).
- [23] Rhodes, G., Proffitt, F., Grady, J. M. & Sumich, A. Facial symmetry and the perception of beauty. *Psychonomic Bulletin & Review* **5**, 659–669 (1998).
- [24] Santos, P. E., Casati, R. & and, P. C. Perception, cognition and reasoning about shadows. *Spatial Cognition & Computation* **18**, 78–85 (2018). URL <https://doi.org/10.1080/13875868.2017.1377204>.

- [25] Landy, M. S. Texture analysis and perception. *The new visual neurosciences* **476**, 639–652 (2013).
- [26] Bereska, L. & Gavves, E. Mechanistic interpretability for ai safety – a review (2024). URL <https://arxiv.org/abs/2404.14082>. 2404.14082.
- [27] Farrell, E., Lau, Y.-T. & Conmy, A. Applying sparse autoencoders to unlearn knowledge in language models (2024). URL <https://arxiv.org/abs/2410.19278>. 2410.19278.
- [28] Bussmann, B., Nabeshima, N., Karvonen, A. & Nanda, N. Learning multi-level features with matryoshka sparse autoencoders (2025). URL <https://arxiv.org/abs/2503.17547>. 2503.17547.
- [29] Park, K., Choe, Y. J. & Veitch, V. The linear representation hypothesis and the geometry of large language models (2024). URL <https://arxiv.org/abs/2311.03658>. 2311.03658.
- [30] Cunningham, H., Ewart, A., Riggs, L., Huben, R. & Sharkey, L. Sparse autoencoders find highly interpretable features in language models (2023). URL <https://arxiv.org/abs/2309.08600>. 2309.08600.
- [31] Dunefsky, J., Chlenski, P. & Nanda, N. Transcoders find interpretable llm feature circuits (2024). URL <https://arxiv.org/abs/2406.11944>. 2406.11944.
- [32] Templeton, A. *et al.* Scaling monosemanticity: Extracting interpretable features from claude 3 sonnet. *Transformer Circuits Thread* (2024). URL <https://transformer-circuits.pub/2024/scaling-monosemanticity/index.html>.
- [33] Huang, K. *et al.* T2i-compbench++: An enhanced and comprehensive benchmark for compositional text-to-image generation (2025). URL <https://arxiv.org/abs/2307.06350>. 2307.06350.
- [34] Kynkäänniemi, T., Karras, T., Laine, S., Lehtinen, J. & Aila, T. Improved precision and recall metric for assessing generative models (2019). URL <https://arxiv.org/abs/1904.06991>. 1904.06991.
- [35] Yang, Y. & Perdikaris, P. Physics-informed deep generative models (2018). URL <https://arxiv.org/abs/1812.03511>. 1812.03511.
- [36] Gerstgrasser, M. *et al.* Is model collapse inevitable? breaking the curse of recursion by accumulating real and synthetic data (2024). URL <https://arxiv.org/abs/2404.01413>. 2404.01413.
- [37] Wadekar, S. N., Chaurasia, A., Chadha, A. & Culurciello, E. The evolution of multimodal model architectures (2024). URL <https://arxiv.org/abs/2405.17927>. 2405.17927.

- [38] Park, K., Choe, Y. J., Jiang, Y. & Veitch, V. The geometry of categorical and hierarchical concepts in large language models (2025). URL <https://arxiv.org/abs/2406.01506>. 2406.01506.
- [39] Bussmann, B., Leask, P. & Nanda, N. Batchtopk sparse autoencoders (2024). URL <https://arxiv.org/abs/2412.06410>. 2412.06410.
- [40] Shi, W. *et al.* Route sparse autoencoder to interpret large language models (2025). URL <https://arxiv.org/abs/2503.08200>. 2503.08200.
- [41] Paulo, G., Shabalin, S. & Belrose, N. Transcoders beat sparse autoencoders for interpretability (2025). URL <https://arxiv.org/abs/2501.18823>. 2501.18823.
- [42] Lindsey, J. *et al.* Sparse crosscoders for cross-layer features and model diffing. *arXiv preprint arXiv:2402.14634* (2024). Accessed June 2025.
- [43] Bricken, T. *et al.* Towards monosemanticity: Decomposing language models with dictionary learning. *Transformer Circuits Thread* (2023). <https://transformer-circuits.pub/2023/monosemantic-features/index.html>.
- [44] Karvonen, A. *et al.* Saebench: A comprehensive benchmark for sparse autoencoders in language model interpretability (2025). URL <https://arxiv.org/abs/2503.09532>. 2503.09532.
- [45] Elhage, N. *et al.* Toy models of superposition (2022). URL <https://arxiv.org/abs/2209.10652>. 2209.10652.
- [46] Lim, Y., Choi, H. & Shim, H. Evaluating image hallucination in text-to-image generation with question-answering (2025). URL <https://arxiv.org/abs/2409.12784>. 2409.12784.
- [47] Kondapaneni, N., Marks, M., Knott, M., Guimaraes, R. & Perona, P. Text-image alignment for diffusion-based perception (2024). URL <https://arxiv.org/abs/2310.00031>. 2310.00031.
- [48] Inoue, N., Furuta, R., Yamasaki, T. & Aizawa, K. Cross-domain weakly-supervised object detection through progressive domain adaptation (2018). URL <https://arxiv.org/abs/1803.11365>. 1803.11365.
- [49] Ramesh, A., Dhariwal, P., Nichol, A., Chu, C. & Chen, M. Hierarchical text-conditional image generation with clip latents (2022). URL <https://arxiv.org/abs/2204.06125>. 2204.06125.
- [50] Kwon, P. & Joo, H. Graspdiffusion: Synthesizing realistic whole-body hand-object interaction (2024). URL <https://arxiv.org/abs/2410.13911>. 2410.13911.

- [51] Lagzian, A., Anumasa, S. & Liu, D. Multi-novelty: Improve the diversity and novelty of contents generated by large language models via inference-time multi-views brainstorming (2025). URL <https://arxiv.org/abs/2502.12700>. 2502.12700.
- [52] Baer, J. *Creativity and divergent thinking: A task-specific approach* (Psychology Press, 2014).
- [53] Chakrabarty, T., Laban, P., Agarwal, D., Muresan, S. & Wu, C.-S. Art or artifice? large language models and the false promise of creativity (2024). URL <https://arxiv.org/abs/2309.14556>. 2309.14556.
- [54] Meng, C. *et al.* Sdedit: Guided image synthesis and editing with stochastic differential equations (2022). URL <https://arxiv.org/abs/2108.01073>. 2108.01073.
- [55] Hristoforu, E. Dall-e 3. <https://huggingface.co/ehristoforu/dalle-3-xl-v2> (2023). Accessed: 2025-03-14.
- [56] Labs, B. F. Flux.1-dev. <https://huggingface.co/black-forest-labs/FLUX.1-dev> (2024). Accessed: 2025-03-14.
- [57] Kwai-Kolors. Kolors-diffusers. <https://huggingface.co/Kwai-Kolors/Kolors-diffusers> (2024). Accessed: 2025-03-14.
- [58] AI, S. Stable cascade: Efficient text-to-image generation in highly compressed latent spaces. <https://huggingface.co/stabilityai/stable-cascade> (2025). Technical Report.
- [59] Chen, H.-Y. *et al.* Contrastive localized language-image pre-training (2025). URL <https://arxiv.org/abs/2410.02746>. 2410.02746.
- [60] Rai, D., Zhou, Y., Feng, S., Saparov, A. & Yao, Z. A practical review of mechanistic interpretability for transformer-based language models (2025). URL <https://arxiv.org/abs/2407.02646>. 2407.02646.
- [61] Xiong, Y., Chang, W.-C., Hsieh, C.-J., Yu, H.-F. & Dhillon, I. Extreme zero-shot learning for extreme text classification (2021). URL <https://arxiv.org/abs/2112.08652>. 2112.08652.
- [62] Carpineto, C. & Romano, G. A survey of automatic query expansion in information retrieval. *Acm Computing Surveys (CSUR)* **44**, 1–50 (2012).
- [63] Johnson, N., Ángel Alexander Cabrera, Plumb, G. & Talwalkar, A. Where does my model underperform? a human evaluation of slice discovery algorithms. <http://dx.doi.org/10.1609/hcomp.v11i1.27548> (2023). Proceedings of the AAAI Conference on Human Computation and Crowdsourcing, Vol. 11, No. 1, pp. 65–76. Association for the Advancement of Artificial Intelligence (AAAI).

- [64] Lin, T.-Y. *et al.* Microsoft coco: Common objects in context (2015). URL <https://arxiv.org/abs/1405.0312>. 1405.0312.
- [65] Plummer, B. A. *et al.* Flickr30k entities: Collecting region-to-phrase correspondences for richer image-to-sentence models (2016). URL <https://arxiv.org/abs/1505.04870>. 1505.04870.
- [66] Sidorov, O., Hu, R., Rohrbach, M. & Singh, A. Textcaps: a dataset for image captioning with reading comprehension (2020). URL <https://arxiv.org/abs/2003.12462>. 2003.12462.
- [67] Agrawal, H. *et al.* nocaps: novel object captioning at scale. <http://dx.doi.org/10.1109/ICCV.2019.00904> (2019). 2019 IEEE/CVF International Conference on Computer Vision (ICCV), IEEE.
- [68] Zhang, L., Rao, A. & Agrawala, M. Adding conditional control to text-to-image diffusion models (2023). URL <https://arxiv.org/abs/2302.05543>. 2302.05543.
- [69] Gao, L. *et al.* Scaling and evaluating sparse autoencoders (2024). URL <https://arxiv.org/abs/2406.04093>. 2406.04093.
- [70] Makhzani, A. & Frey, B. k-sparse autoencoders (2014). URL <https://arxiv.org/abs/1312.5663>. 1312.5663.
- [71] Radford, A. *et al.* Learning transferable visual models from natural language supervision (2021). URL <https://arxiv.org/abs/2103.00020>. 2103.00020.
- [72] Sun, X., Engels, J. & Tegmark, M. High frequency latents are features, not bugs. <https://openreview.net/forum?id=IT5fRjnGr0> (2025). Sparsity in LLMs (SLLM): Deep Dive into Mixture of Experts, Quantization, Hardware, and Inference.
- [73] Minegishi, G., Furuta, H., Iwasawa, Y. & Matsuo, Y. Rethinking evaluation of sparse autoencoders through the representation of polysemous words (2025). URL <https://arxiv.org/abs/2501.06254>. 2501.06254.
- [74] Oquab, M. *et al.* Dinov2: Learning robust visual features without supervision (2024). URL <https://arxiv.org/abs/2304.07193>. 2304.07193.
- [75] Anthropic. Claude haiku. <https://www.anthropic.com/index/claude> (2024). Accessed: 2025-05-04.
- [76] Meta AI. Llama 3 instruct. <https://ai.meta.com/llama/> (2024). Accessed: 2025-05-04.
- [77] Luo, Y. *et al.* Llm as dataset analyst: Subpopulation structure discovery with large language model (2024). URL <https://arxiv.org/abs/2405.02363>. 2405.02363.

- [78] Luo, Y., Tang, Y., Shen, C., Zhou, Z. & Dong, B. Prompt engineering through the lens of optimal control (2023). URL <https://arxiv.org/abs/2310.14201>. 2310.14201.
- [79] Hinton, G., Vinyals, O. & Dean, J. Distilling the knowledge in a neural network (2015). URL <https://arxiv.org/abs/1503.02531>. 1503.02531.
- [80] Xu, L., Xie, H., Qin, S.-Z. J., Tao, X. & Wang, F. L. Parameter-efficient fine-tuning methods for pretrained language models: A critical review and assessment (2023). URL <https://arxiv.org/abs/2312.12148>. 2312.12148.

A. Qualitative Examples of LanSE Neurons

In this section, we provide qualitative examples of the interpretable visual patterns used in our evaluation framework, LanSE. These visualizations contain individual features that encodes meaningful explanations and the set of images that can activate them, including both photos and generated images.

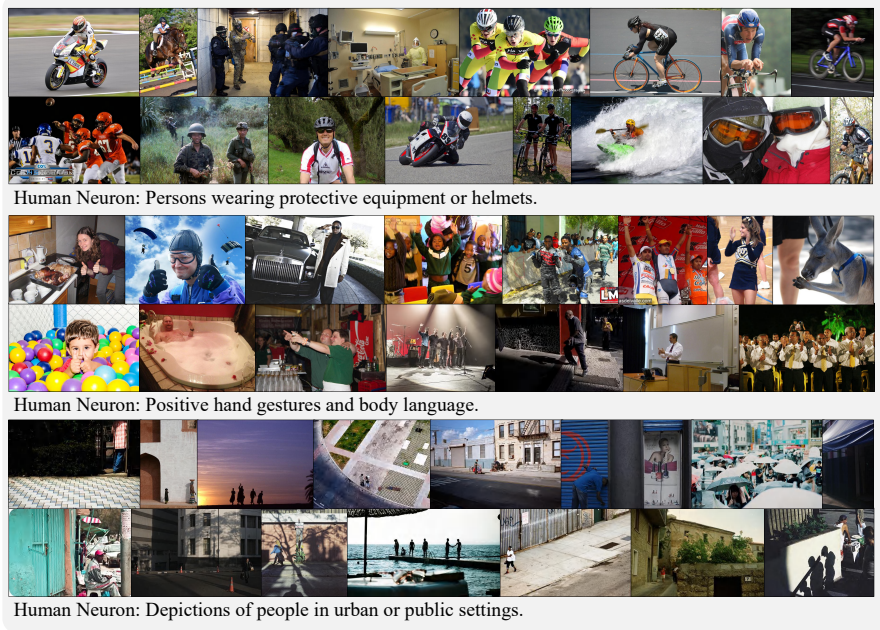


Fig. 12: Feature examples for the human subgroup of prompt match.



Fig. 13: Feature examples for the animal subgroup of prompt match.



Object Neuron: Fast food, snacks, or other prepared foods.



Object Neuron: Musical instruments and musical performance.

Fig. 14: Feature examples for the object subgroup of prompt match.



Activity Neuron: Soccer-related images, including soccer players, balls, and events.



Activity Neuron: Workers engaged in manual labor and industrial activities.

Fig. 15: Feature examples for the activity subgroup of prompt match.



Environment Neuron: Urban, gritty, public street scenes with graffiti, signs, and people in a city environment.



Environment Neuron: Street scenes with traffic signals, crosswalks, and pedestrians.

Fig. 16: Feature examples for the environment subgroup of prompt match.



Style Neuron: The images are unrealistic because they are stylized illustrations or digital art, with an abstract or exaggerated visual representation.



Style Neuron: The images have an artistic, stylized aesthetic that departs from photorealistic representation, creating an intentionally unrealistic and imaginative visual perception.



Style Neuron: The images have a painting-like or digital art style, which intentionally gives them an unrealistic and fantastical appearance.

Fig. 17: Feature examples for the style subgroup of visual realism.



Artifact Neuron: The images are unrealistic due to excessive lighting, distorted proportions, and unnatural color palettes that do not match real-world classrooms.



Artifact Neuron: The images are unrealistic because they contain technical details or text that are not part of the actual coin design.



Artifact Neuron: The images feature an overabundance of the letter 'M', which creates an unrealistic and artificial visual representation.



Artifact Neuron: The images contain unrealistic details or combinations that do not exist in the real world.

Fig. 18: Feature examples for the artifact subgroup of visual realism.

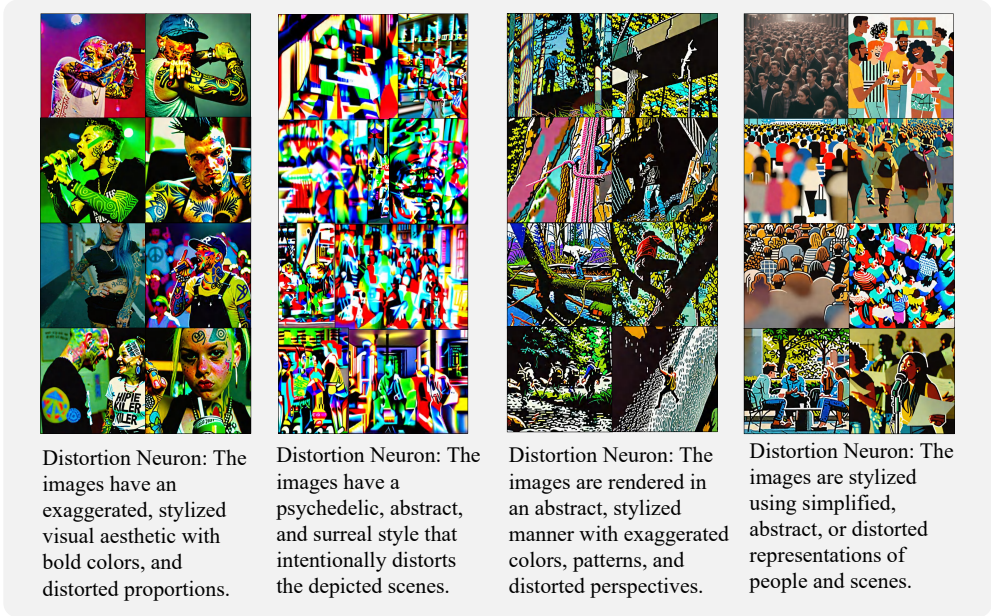


Fig. 19: Feature examples for the distortion subgroup of physical plausibility.

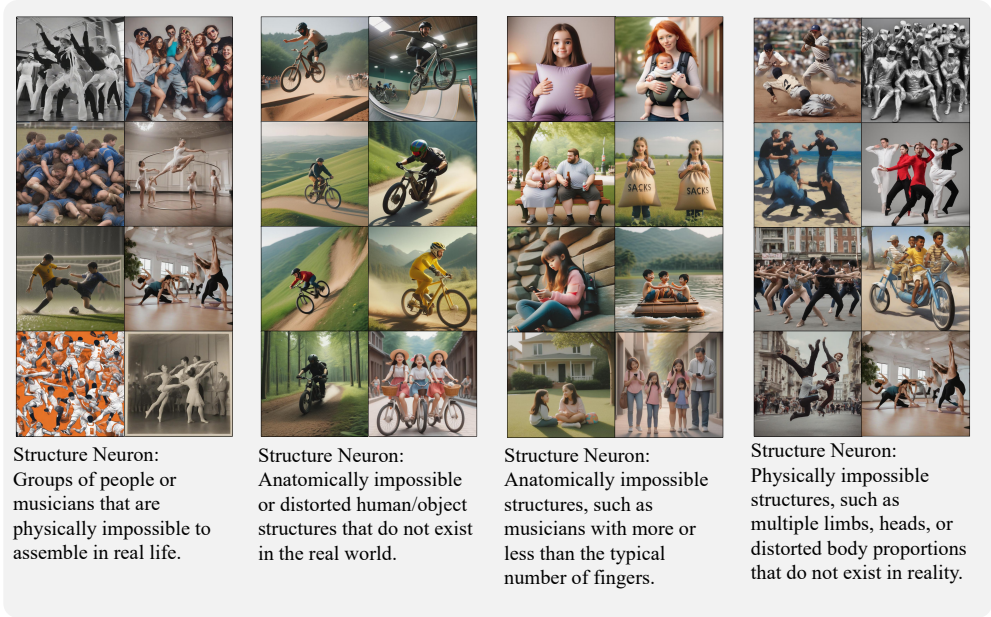


Fig. 20: Feature examples for the structure subgroup of physical plausibility.

B. Qualitative Examples of Image-caption Pairs and Activated Neurons

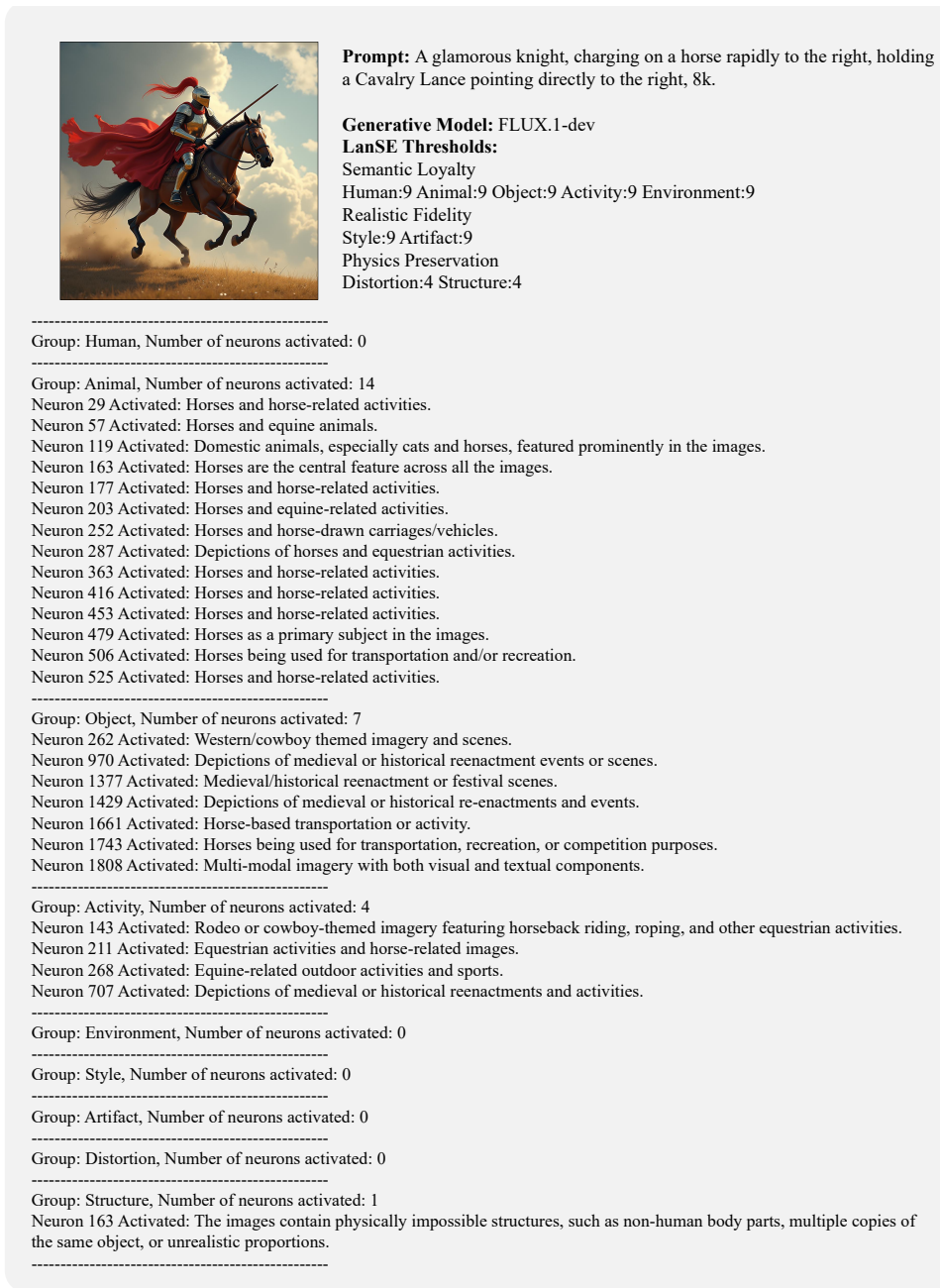


Fig. 21: Image example and the LanSE neurons it highly activates.



Prompt: There are two women crossing the street in front of two buses.

Generative Model: Kolors-diffusers

LanSE Thresholds:

Semantic Loyalty
 Human:9 Animal:9 Object:9 Activity:9 Environment:9
 Realistic Fidelity
 Style:9 Artifact:9
 Physics Preservation
 Distortion:4 Structure:4

 Group: Human, Number of neurons activated: 3

Neuron 224 Activated: Scenes depicting human figures, individuals or groups, in various settings and contexts.
 Neuron 244 Activated: Depictions of human subjects and social interactions in urban, public, and domestic settings.
 Neuron 499 Activated: Depiction of human figures and interactions in various settings.

 Group: Animal, Number of neurons activated: 0

 Group: Object, Number of neurons activated: 8 (4 Omitted for Display)

Neuron 463 Activated: Visual art and creative representations.
 Neuron 585 Activated: Representations of various cultural, social, or artistic elements.
 Neuron 634 Activated: Transportation-related elements in urban settings.
 Neuron 686 Activated: Transportation by bus.

 Group: Activity, Number of neurons activated: 0

 Group: Environment, Number of neurons activated: 1

Neuron 136 Activated: Urban environment with various transportation-related features.

 Group: Style, Number of neurons activated: 4 (1 Omitted for Display)

Neuron 11 Activated: The images exhibit a stylized, non-photorealistic aesthetic, likely generated or edited using artificial techniques to achieve an unrealistic visual effect.
 Neuron 62 Activated: The images are in a stylized, artistic illustration style that deviates from photorealistic representation, creating an unrealistic yet visually compelling depiction.
 Neuron 118 Activated: The images are stylized using bold, geometric shapes, vibrant colors, and simplified forms to create an abstract, illustrative aesthetic.

 Group: Artifact, Number of neurons activated: 17 (13 Omitted for Display)

Neuron 94 Activated: The images exhibit unrealistic features, such as disproportionate elements, unnatural poses, or improbable settings, that deviate from realistic representation.
 Neuron 139 Activated: The images exhibit various visual inconsistencies, such as unrealistic proportions, disproportionate elements, and lack of proper lighting and shadows, making them appear unrealistic.
 Neuron 173 Activated: The images appear unrealistic due to various inconsistencies, such as disproportionate features, unnatural poses, and implausible scene compositions.
 Neuron 191 Activated: The images are unrealistic due to exaggerated or unnatural details, compositions, and lighting that do not match real-world observations.

 Group: Distortion, Number of neurons activated: 0

 Group: Structure, Number of neurons activated: 7 (4 Omitted for Display)

Neuron 47 Activated: The images depict physically impossible structures, such as additional limbs, unrealistic body proportions, or multiple identical individuals in one frame.
 Neuron 48 Activated: The images depict human bodies or scenes that do not conform to natural anatomical or physical constraints.
 Neuron 220 Activated: The images contain unrealistic anatomical features and object arrangements that do not conform to the physical constraints of the real world.

Fig. 22: Image example and the LanSE neurons it highly activates.



Prompt: A girl in a gray shirt is throwing her hands up .

Generative Model: DALLE3

LanSE Thresholds:

Semantic Loyalty

Human:7 Animal:7 Object:7 Activity:7 Environment:7

Realistic Fidelity

Style:9 Artifact:9

Physics Preservation

Distortion:4 Structure:4

Group: Human, Number of neurons activated: 7

Neuron 2 Activated: Positive hand gestures and body language.

Neuron 97 Activated: Human faces and figures in indoor and outdoor settings.

Neuron 116 Activated: Most of the images depict females, such as young girls or women, in various situations and environments.

Neuron 164 Activated: Presence of human faces and figures in the images.

Neuron 250 Activated: Presence of a young female/girl in the images.

Neuron 527 Activated: Expressive facial expressions depicting strong emotions.

Neuron 670 Activated: Individuals dressed in Halloween or horror-themed costumes, often with exaggerated or disturbing makeup and attire.

Group: Animal, Number of neurons activated: 0

Group: Object, Number of neurons activated: 5

Neuron 823 Activated: Photography and capturing images.

Neuron 1067 Activated: Expressing emotional states, particularly crying or distress, in human and animal subjects.

Neuron 1600 Activated: Everyday objects and scenes depicted in the images.

Neuron 1698 Activated: Visual media depicting various subjects and scenes.

Neuron 1808 Activated: Multi-modal imagery with both visual and textual components.

Group: Activity, Number of neurons activated: 3

Neuron 169 Activated: Images depicting human activities and experiences.

Neuron 532 Activated: Hands raised or gestures made with hands in the images.

Neuron 755 Activated: Visual depictions of human activities, interactions, and environments.

Group: Environment, Number of neurons activated: 1

Neuron 91 Activated: Scenes depicting various environments and settings, including indoor and outdoor scenes, weather conditions, and modes of transportation.

Group: Style, Number of neurons activated: 0

Group: Artifact, Number of neurons activated: 2

Neuron 27 Activated: The images appear unrealistic due to various inconsistencies, such as unnatural proportions, lighting, or physical interactions.

Neuron 620 Activated: The images are unrealistic due to the unnatural or exaggerated human poses, expressions, or interactions with the environment.

Group: Distortion, Number of neurons activated: 0

Group: Structure, Number of neurons activated: 6 (3 Omitted for Display)

Neuron 49 Activated: The images depict physically impossible scenarios, such as multiple limbs, body parts, or unnatural poses that cannot be achieved in the real world.

Neuron 92 Activated: The images depict exaggerated, surreal, and fantastical representations of human and animal forms that do not conform to natural anatomical structures.

Neuron 163 Activated: The images contain physically impossible structures, such as non-human body parts, multiple copies of the same object, or unrealistic proportions.

Fig. 23: Image example and the LanSE neurons it highly activates.



Prompt: A backpacker in the mountains wearing an american flag.

Generative Model: stable-diffusion-3.5-medium

LanSE Thresholds:

Semantic Loyalty
 Human:7 Animal:7 Object:7 Activity:7 Environment:7
 Realistic Fidelity
 Style:9 Artifact:9
 Physics Preservation
 Distortion:4 Structure:4

 Group: Human, Number of neurons activated: 1

Neuron 97 Activated: Human faces and figures in indoor and outdoor settings.

 Group: Animal, Number of neurons activated: 0

 Group: Object, Number of neurons activated: 14 (4 Omitted for Display)

- Neuron 16 Activated: Representations of American patriotism and national identity.
- Neuron 35 Activated: Representation of national or cultural identity through flags and patriotic imagery.
- Neuron 258 Activated: American military and patriotic imagery and symbols.
- Neuron 541 Activated: Imagery and symbols representing the United States of America.
- Neuron 571 Activated: Outdoor recreational and geographic landmarks.
- Neuron 687 Activated: Military or military-related imagery and themes.
- Neuron 776 Activated: Patriotic American imagery and symbolism.
- Neuron 867 Activated: Images depicting various objects, scenes, and situations related to human daily life and activities.
- Neuron 913 Activated: Patriotic and American-themed imagery.
- Neuron 980 Activated: Flags representing various countries or nationalities.

 Group: Activity, Number of neurons activated: 7

- Neuron 170 Activated: Snow sports and skiing activities in snowy mountain environments.
- Neuron 198 Activated: Mountainous outdoor scenes with people engaged in hiking or climbing activities.
- Neuron 258 Activated: Mountain climbing and outdoor activities in snowy, mountainous landscapes.
- Neuron 277 Activated: Outdoor recreational activities and camping scenes.
- Neuron 319 Activated: Outdoor recreational activities and wilderness exploration in mountainous, rocky terrain.
- Neuron 330 Activated: Outdoor hiking and exploration activities in natural environments.
- Neuron 600 Activated: People hiking and exploring natural outdoor environments.

 Group: Environment, Number of neurons activated: 8

- Neuron 8 Activated: Outdoor scenes featuring mountains, snow, and winter landscapes.
- Neuron 40 Activated: Mountainous landscapes and natural outdoor settings.
- Neuron 54 Activated: Outdoor nature scenes with people interacting with and exploring mountainous, rocky, or snowy environments.
- Neuron 120 Activated: Nature and wilderness scenes in forested environments.
- Neuron 143 Activated: Mountainous landscapes with snow-capped peaks.
- Neuron 202 Activated: Mountainous landscapes with people engaged in outdoor activities.
- Neuron 208 Activated: Mountainous landscapes and natural environments.
- Neuron 380 Activated: Outdoor hiking and trekking in natural environments.

 Group: Style, Number of neurons activated: 0

 Group: Artifact, Number of neurons activated: 0

 Group: Distortion, Number of neurons activated: 0

 Group: Structure, Number of neurons activated: 0

Fig. 24: Image example and the LanSE neurons it highly activates.

C. LMM Analysis Prompts

In this Appendix, we list the prompts we have used in our pipelines.

We use the following prompt to summarize the common features among one given neuron and its corresponding subpopulation that can highly activate it.

Feature Summarization Prompt

You are an expert in multimodal feature analysis.
{(image)(caption)(image)(caption)...}
Analyze the commonalities among these samples. Identify: If there exist one common feature that is possessed by all the instances. Summarize and output exactly one feature, for example: '[Commonality: Animal wildlife in natural habitats]' and '[Commonality: Strawberry-based dessert or dish]'. Only answer in general, do not analyze each image one by one, only generate one single concise phrase. Start answer with '[Commonality:'. End with ']'

We use the following prompt to assign the prompt match neurons to their corresponding neuron groups, human, animal, object, activity or environment.

Semantics Feature Categorization Prompt

You are a helpful assistant categorizing image features into exactly one of the following groups: "[human, animal, object, activity, environment]."
Given the commonality description: commonality, which of the five categories does it best belong to? Please answer with a single word from this list: [human, animal, object, activity, environment]. Wrap your answer in [].

We use the following prompt to assign the visual realism neurons to their corresponding neuron groups, style or artifact.

Realism Feature Categorization Prompt

Here is a set of image samples along with their captions:
{(image)(caption)(image)(caption)...}
They are probably unrealistic for certain reason.
One type of reason is the style of the images is intended to be unrealistic, like cartoonish or stamp-like, or painting-like. Another type of reason is visual artifact, like a photo of a real scene but is unrealistic because of the violation of conventions or details.
Please answer in the following format: [Style, Explanation: {explanation}] or [Artifact, Explanation: {explanation}] Only give me one answer that is common to all the images and can explain all of them, the explanation should be as short as possible, no more than 20 words.

We use the following prompt to assign the physical plausibility neurons to their corresponding neuron groups, distortion or structure.

Physics Feature Categorization Prompt

Here is a set of image samples along with their captions:

{(image)(caption)(image)(caption)...}

They all possess one common pattern that make them physically impossible.

One type of features is the distortion of the object surface, like distorted faces or blurred surfaces. Another type of features is the structure of the object, like more than six fingers on a hand, one head on a single body or three legs on a single human.

What is the common pattern that make them physically impossible? Please answer in the following format: [Distortion, Explanation: {explanation}] or [Structure, Explanation: {explanation}] Only give me one answer that is common to all the images and can explain all of them, the explanation should be as short as possible, no more than 20 words.

D. Method Extention

Certain failure modes in generative models, such as physics violations (e.g., distorted limbs, extra fingers), are both rare and critical, yet difficult to discover through random sampling. To address this, we develop an interactive human-in-the-loop framework that enables targeted pattern discovery at scale while reducing human annotation cost, as shown in Figure 25.

Motivation

While LanSE neurons are primarily derived from large-scale, sparsity-driven interpretability modules, the discovery of interpretable features depends on the availability of sufficiently frequent patterns in the training data. However, physics-related errors, such as anatomically impossible structures, are often of low frequency and hard to detect without guidance. Exhaustively humanly reviewing 250,000+ images is infeasible. Therefore, we build an iterative system that leverages weak supervision from lightweight classifiers to bootstrap the collection of relevant samples.

Interactive Data Curation Pipeline

We begin by collecting an initial seed dataset of 300 images containing known physics violations, along with an equal number of negative samples. Human annotators manually label each image as exhibiting physics-consistent or physics-violating content. These labels are then used to train a lightweight two-layer binary classifier on CLIP image embeddings. The classifier architecture is:

- Input: CLIP image embedding.
- Hidden: Fully connected ReLU layer.
- Output: Sigmoid activation for binary label (violation / no violation).

Once trained, this classifier is used to scan the full image dataset and flag potentially erroneous images. These flagged samples are then sent to human annotators for relabeling. The updated labels are added to the training pool, and the classifier is retrained. This bootstrapping process continues iteratively, improving both coverage and precision of error discovery.

This approach enables the discovery of rare but critical patterns in a scalable manner, cutting down the annotation cost by an order of magnitude compared to exhaustive search.

Integration into LanSE

After sufficient labeled data is accumulated through this pipeline, we train a sparse transcoder on the intermediate representations of the two-layer classifier. Specifically, we extract the hidden activations and train a sparse autoencoder over them using the same top-k sparsity constraints as in the main pipeline.

This generates a new set of interpretable neurons, which are curated via the same LMM-based explanation and categorization pipeline. These neurons form the distortion and structure groups within LanSE’s physical plausibility dimension. By

grounding these rare pattern detectors in both language and visual representations, LanSE gains the capacity to diagnose physics violations that would otherwise remain underrepresented.

One thing should be mentioned is that this interactive feature discovery pipeline is based on the intuition that task-related patterns are more prevalent in task-related models. In particular, patterns that is related to physics violations are more likely to be discovered in a model that is used to classify images according to whether they have physics violations or not.

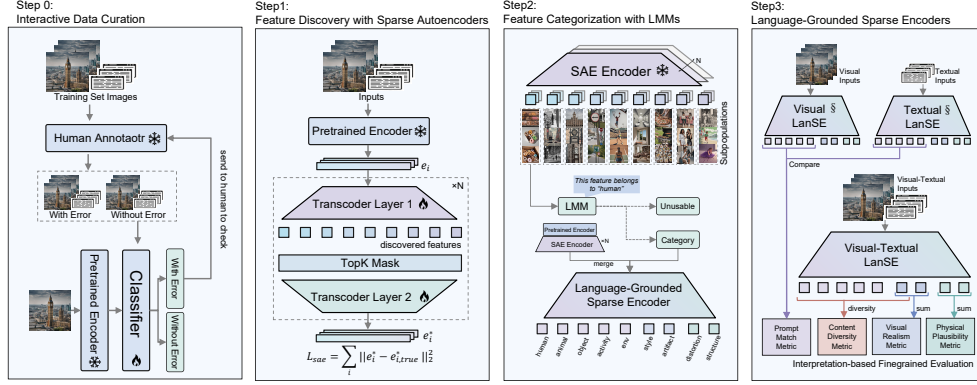


Fig. 25: The general pipeline of our extended method used for discovering monosemantic neurons that selectively respond to targeted semantics (physics violations).

E. Metrics Extention

Here are our mathematical definition and calculative derivations of the four defined metrics, prompt match, visual realism, physical plausibility and content diversity.

Prompt Match: This metric captures semantic mismatches between generated images and prompts, such as missing or extraneous content. Grouped into five semantic categories, the metric is computed as the average number of neurons that diverge across modalities. Higher values indicate less semantic alignments. **prompt** can be altered with **human**, **animal**, **object**, **activity**, or **environment**.

$$\begin{aligned} \mathcal{M}_{\text{prompt}}(\mathcal{X}, \mathcal{Y}) &= \mathbb{E}_{\mathbf{D}} \|\mathbf{N}_{\text{prompt}}^{\mathbf{v}}(\mathbf{x}) \oplus \mathbf{N}_{\text{prompt}}^{\mathbf{t}}(\mathbf{y})\|_1 \\ &= \frac{1}{N} \sum_{\mathbf{D}} \|\mathbf{I}\{\mathbf{S}_{\text{prompt}}^{\mathbf{v}}(\mathbf{x}_i) > \tau\} - \mathbf{I}\{\mathbf{S}_{\text{prompt}}^{\mathbf{t}}(\mathbf{y}_i) > \tau\}\|_1. \end{aligned} \quad (8)$$

Visual Realism: This metric measures visual patterns that make the images unrealistic, such as special artistic styles or visual artifacts. Neurons are grouped into style and artifact subcategories. Higher value reflects more deviation from realistic appearances. We differentiate the style group and the artifact group because some artistic styles can be intentional. Higher scores indicate the images are more unrealistic. **real** can be altered with **style** or **artifact**.

$$\mathcal{M}_{\text{real}}(\mathcal{X}, \mathcal{Y}) = \mathbb{E}_{\mathbf{D}} \|\mathbf{N}_{\text{real}}(\mathbf{x}, \mathbf{y})\|_1 = \frac{1}{N} \sum_{\mathbf{D}} \|\mathbf{I}\{\mathbf{S}_{\text{real}}(\mathbf{x}_i, \mathbf{y}_i) > \tau\}\|_1. \quad (9)$$

Physical Plausibility: This metric detects intuitively erroneous patterns that can make an image physically implausible and unwanted, including distortions of the object surfaces or implausible structures like erroneous anatomies. Higher value suggests more errors generated. **phy** can be altered with **distortion** or **structure**.

$$\mathcal{M}_{\text{phy}}(\mathcal{X}, \mathcal{Y}) = \mathbb{E}_{\mathbf{D}} \|\mathbf{N}_{\text{phy}}^{\mathbf{v}}(\mathbf{x})\|_1 = \frac{1}{N} \sum_{\mathbf{D}} \|\mathbf{I}\{\mathbf{S}_{\text{phy}}(\mathbf{x}_i) > \tau\}\|_1. \quad (10)$$

Content Diversity: This metric measures how diverse a generative model’s outputs are. Neurons in the five prompt match groups and the style group are considered as content neurons, and based on them we compute the average divergence of neurons given two image samples. Higher value suggests better model diversity. Expectation is computed on images $((\mathbf{x}_i, \mathbf{y}_i))$ in the distribution with $|\mathbf{N}_{\text{con}}(\mathbf{x}_i, \mathbf{y}_i)| \neq 0$. **con** can be altered with **human**, **animal**, **object**, **activity**, **environment** or **style**.

$$\begin{aligned} \mathcal{M}_{\text{con}}(\mathcal{X}, \mathcal{Y}) &= \mathbb{E}_{\mathbf{D}} \frac{\|\mathbf{N}_{\text{con}}(\mathbf{x}_i, \mathbf{y}_i) \oplus \mathbf{N}_{\text{con}}(\mathbf{x}_j, \mathbf{y}_j)\|_1}{\|\mathbf{N}_{\text{con}}(\mathbf{x}_i, \mathbf{y}_i)\|_1 \cdot \|\mathbf{N}_{\text{con}}(\mathbf{x}_j, \mathbf{y}_j)\|_1} \\ &= \frac{1}{N} \sum_{\mathbf{D}} \frac{1 - \|\mathbf{I}\{\mathbf{S}_{\text{con}}(\mathbf{x}_i, \mathbf{y}_i) > \tau\} \cdot \mathbf{I}\{\mathbf{S}_{\text{con}}(\mathbf{x}_j, \mathbf{y}_j) > \tau\}\|_1}{\|\mathbf{I}\{\mathbf{S}_{\text{con}}(\mathbf{x}_i, \mathbf{y}_i) > \tau\}\|_1 \cdot \|\mathbf{I}\{\mathbf{S}_{\text{con}}(\mathbf{x}_j, \mathbf{y}_j) > \tau\}\|_1}. \end{aligned} \quad (11)$$

F. Human Evaluation Protocols

In this section, we detail the procedures we conduct for the human evaluations. Our human evaluation protocol for LanSE’s feature accuracy is shown in Figure 26. Human annotators are trained and tasked to identify if the image generally matches with the interpretation from LanSE. We release the human evaluation website for transparency: <https://512d-223-109-239-18.ngrok-free.app/>.

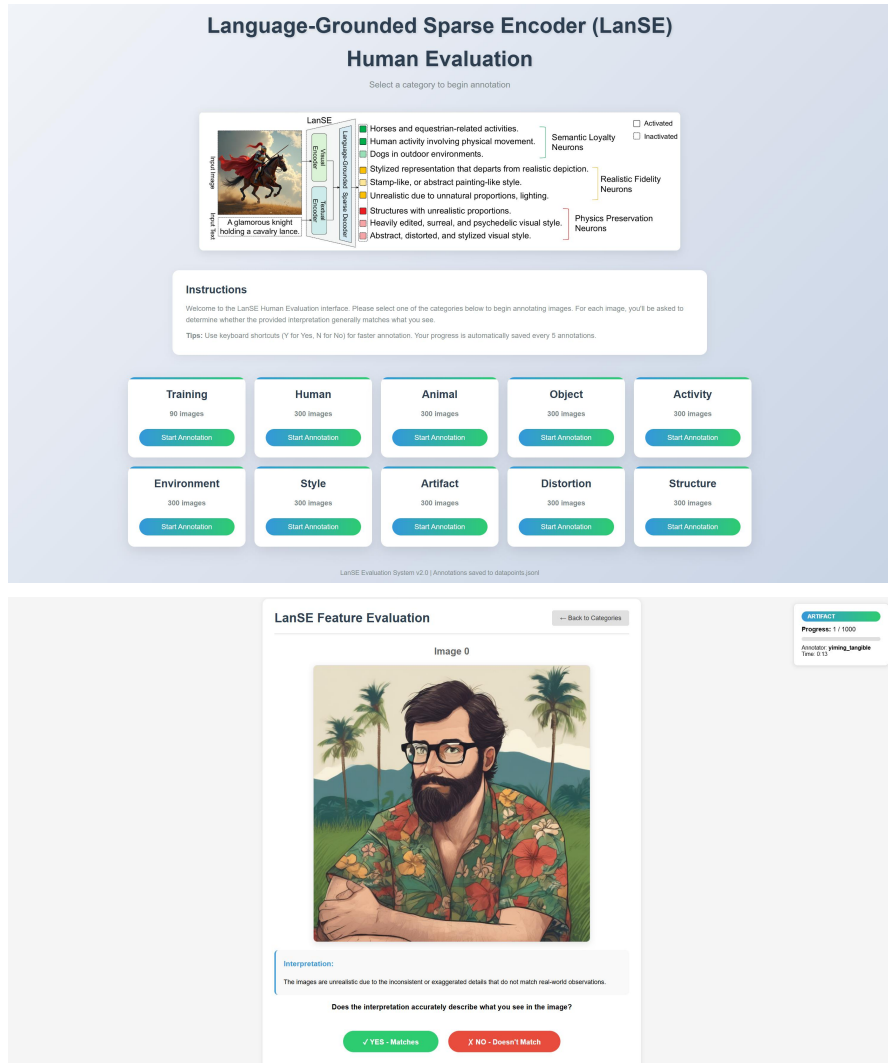


Fig. 26: A demonstration of our human evaluation web interface. Human annotators are tasked to identify if the image generally matches with the LanSE interpretations.

G. The Choice of LanSE Neuron Groups

The organization of LanSE neurons into nine specific groups reflects fundamental aspects of how practitioners evaluate generated images. When prompting a generative model, users typically assess outputs along three primary dimensions:

1. Semantic Alignment: Does the generated image match the prompt? To evaluate this, we need to detect what semantic content appears in images versus what was requested in text. We organize prompt match neurons into five categories that comprehensively cover visual content:

- **Human:** Detects people, faces, and human-related attributes
- **Animal:** Identifies animals and their characteristics
- **Object:** Recognizes man-made objects and items
- **Activity:** Captures actions, events, and dynamic scenes
- **Environment:** Identifies settings, locations, and backgrounds

2. Visual Realism: Does the image look realistic? Unrealistic patterns fall into two distinct categories:

- **Style:** Artistic styles or rendering techniques that deviate from photorealism (e.g., cartoon, watercolor)
- **Artifact:** Unintended visual artifacts that compromise image quality (e.g., noise, compression artifacts)

3. Physical Plausibility: Does the image contain patterns that make it unusable? Critical errors that violate physical constraints include:

- **Distortion:** Surface-level distortions and warping effects
- **Structure:** Anatomically impossible structures (e.g., extra fingers, impossible object configurations)

This hierarchical organization enables LanSE to provide comprehensive evaluation coverage while maintaining clear interpretability. Each group addresses specific failure modes that practitioners encounter, making the evaluation results actionable for model improvement.

H. Ablation Studies

To understand the influences of the hyperparameters to the LanSE framework, we conduct two ablation studies on the activation threshold, τ . We evaluate how the number of activated interpretable neurons changes with varying thresholds and how the accuracy of signals in each group change with varying thresholds.

Metrics v.s. the Activation Threshold τ We tune the activation threshold used for the LanSE neurons and collect all our defined metrics. The results are listed in Figure 28 and Figure 27.

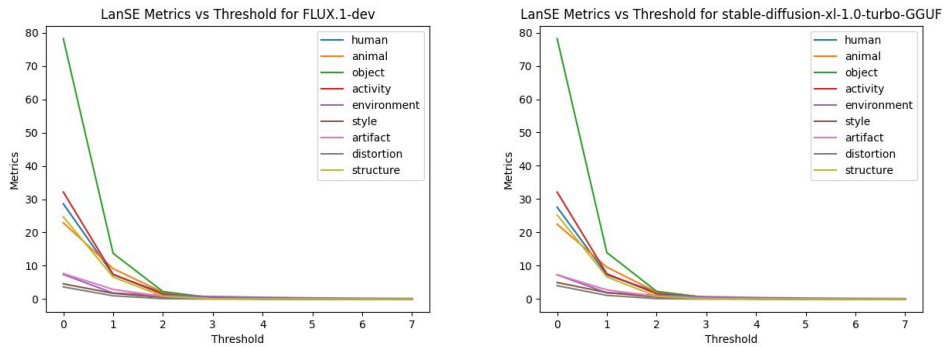


Fig. 27: LanSE metrics varying according to the threshold choices for two models. Higher thresholds mean the neurons are less likely activated and leads to smaller metric values.

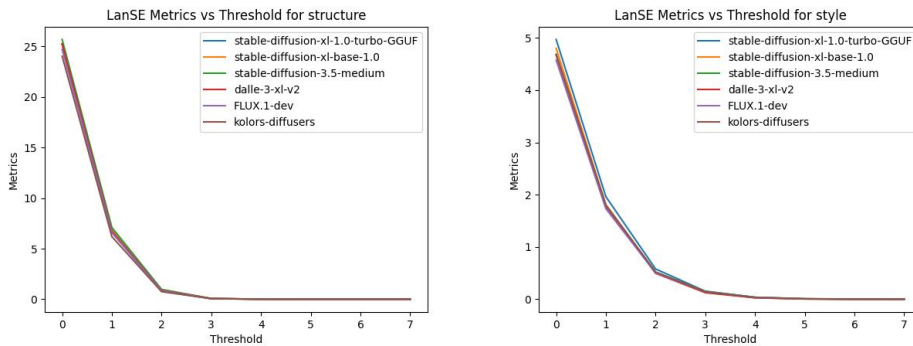


Fig. 28: LanSE metrics varying according to the threshold choices for two groups. Higher thresholds mean the neurons are less likely activated and leads to smaller metric values. Lower metrics gives better contrast between models, making it easier to distinguish them.

Accuracies v.s. the Activation Threshold τ We tune the activation threshold used for the LanSE neurons and utilize an LMM to evaluate the ratio of images that can activate the neurons generally match the natural language interpretations. The results are listed in Figure 29.

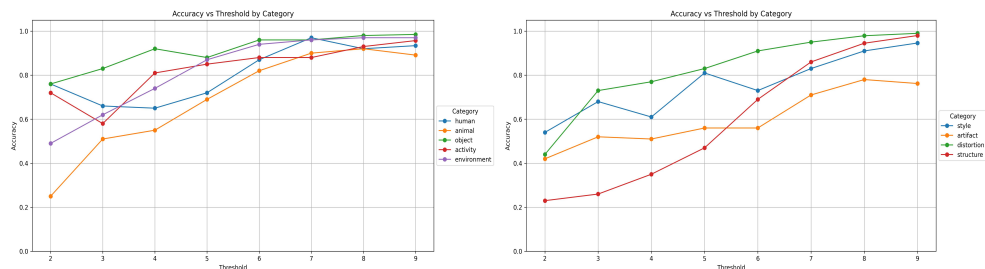


Fig. 29: LanSE’s signal accuracies varying according to the threshold choices. Higher thresholds means stricter constraints on the neural activations and therefore higher accuracies for the signals.

We use the following prompt for the evaluation of neuron accuracies.

Accuracy Evaluation Prompt

{(image)(explanation)}.

Above is one image and one explanation of the image. Please check if the explanation generally matches the image. Answer only with "yes" or "no".

I. Limitations

Language-Describable Patterns Only. LanSE inherently evaluates only patterns that can be described in natural language, introducing an anthropocentric bias. Subtle failures or perceptually important patterns that lack linguistic representations may escape detection. While we argue this aligns with practical requirements, as humans primarily care about describable failures, this constraint limits our ability to capture the full spectrum of possible generation errors.

Dependence on Base Encoder Quality. Our framework’s effectiveness is fundamentally limited by the representations learned by the underlying encoders (CLIP in our implementation). Known biases in CLIP, such as texture bias and limited cultural diversity, propagate through to LanSE evaluations. Future work should explore ensemble approaches using diverse encoders to mitigate these inherited biases.

Computational and Scalability Constraints. Training 250 sparse autoencoders and curating 3.75 million candidate neurons requires substantial computational resources. While our filtering reduces this to 5,309 neurons, the initial discovery phase may be prohibitive for some applications. Additionally, the current architecture scales linearly with the number of evaluation aspects, potentially limiting real-time applications.

Evaluation Scope and Coverage. Our framework currently addresses four evaluation dimensions, leaving important aspects like aesthetic quality, cultural appropriateness, and implicit social biases unmeasured. Additionally, certain visual patterns, particularly those involving complex spatial relationships or subtle emotional expressions, may be underrepresented in our discovered features, creating evaluation blind spots.

Context-Insensitive Evaluation. LanSE cannot distinguish between intentional stylistic choices and undesirable artifacts without additional context. A distorted perspective might be an artistic choice in one context but a failure in another. This limitation is particularly relevant for creative applications where "errors" may be features. Future work should explore incorporating user intent or task specifications into the evaluation pipeline.

Static Feature Set. Our current implementation uses a fixed set of discovered features, which may become outdated as generative models evolve and develop new failure modes. While our LMM-based curation pipeline provides some flexibility, adapting to entirely new types of generation errors requires retraining the underlying sparse autoencoders.